

# 1 **Dynamic estimation of the attentional field from 2 visual cortical activity**

3  
4 **Ilona M. Bloem<sup>1,2\*</sup>, Leah Bakst<sup>1\*</sup>, Joseph T. McGuire<sup>1</sup>, Sam Ling<sup>1</sup>**

5  
6 <sup>1</sup> Department of Psychological & Brain Sciences, Boston University, Boston, USA

7 <sup>2</sup> Department of Computational Cognitive Neuroscience and Neuroimaging, Netherlands  
8 Institute for Neuroscience, Amsterdam, Netherlands & Spinoza Centre for Neuroimaging,  
9 Amsterdam, Netherlands

10  
11 \* These authors provided equal contribution

12  
13 Correspondence should be addressed to Sam Ling (samling@bu.edu).

14  
15 Abbreviated title: Dynamical estimation of the attentional field

16  
17  
18  
19  
20 Number of pages: 28

21 Number of figures: 7

22 Number of words for:

23 Abstract: 232

24 Introduction: 653

25 Discussion: 1446

26 Methods: 2505

27  
28 The authors declare no competing financial interests.

29  
30 Acknowledgements: This work was supported by National Science Foundation grants  
31 SMA-1809071, BCS-1625552, and BCS-1755757, National Institutes of Health grants  
32 F32-EY029134, R01-EY028163, and R01-MH126971, Office of Naval Research grant  
33 N00014-17-1-2304, and the Center for Systems Neuroscience Postdoctoral Fellowship  
34 at Boston University. The content of this paper does not necessarily represent the official  
35 views of the funding agencies.

36  
37 Author contributions: Conceptualization, Methodology & Writing – Review & Editing  
38 I.M.B., L.B., J.T.M., S.L.; Investigation, Analysis, Visualization, & Writing – Original Draft,  
39 I.M.B. & L.B.; Resources & Supervision, J.T.M & S.L.; Funding Acquisition L.B., J.T.M.,  
40 S.L.

## 1 Abstract

2 Navigating around the world, we must adaptively allocate attention to our surroundings  
3 based on anticipated future stimuli and events. This allocation of spatial attention boosts  
4 visuocortical representations at attended locations and locally enhances perception.  
5 Indeed, spatial attention has often been analogized to a “spotlight” shining on the item  
6 of relevance. Although the neural underpinnings of the locus of this attentional spotlight  
7 have been relatively well studied, less is known about the size of the spotlight: to what  
8 extent can the attentional field be broadened and narrowed in accordance with  
9 behavioral demands? In this study, we developed a paradigm for dynamically estimating  
10 the locus and spread of covert spatial attention, inferred from visuocortical activity using  
11 fMRI in humans. We measured BOLD activity in response to an annulus while  
12 participants (4 female, 4 male) used covert visual attention to determine whether more  
13 numbers or letters were present in a cued region of the annulus. Importantly, the width  
14 of the cued area was systematically varied, calling for different sizes of the attentional  
15 spotlight. The deployment of attention was associated with an increase in BOLD activity  
16 in corresponding retinotopic regions of visual areas V1–V3. By modeling the  
17 visuocortical attentional modulation, we could reliably recover the cued location, as well  
18 as a broadening of the attentional modulation with wider attentional cues. This modeling  
19 approach offers a useful window into the dynamics of attention and spatial uncertainty.

## 20 Significance Statement

21 This study explores whether spatial attention can dynamically adapt by shifting and  
22 broadening the attentional field. While previous research has focused on the modulation  
23 of neural responses at attended locations, less is known about how the size of the  
24 attentional field is represented within visual cortex. Using fMRI, we developed a novel  
25 paradigm to estimate the spatial tuning of the attentional field and demonstrate that we  
26 were able to recover both the location as well as the width of the attentional field. Our  
27 findings offer new insights into the neural mechanisms underlying the deployment of  
28 spatial attention, contributing to a deeper understanding of how spatial attention  
29 supports visual perception.  
30

## 1 Introduction

2 We bounce attention around all the time. Take, for instance, when we're monitoring  
3 oncoming traffic while driving. It isn't sufficient to attend to the single most likely source  
4 of traffic. Instead, attention adaptively broadens and narrows to cover the anticipated  
5 spatial distribution of relevant events. The need to spread attention across different  
6 swaths of the visual field is driven, to a large degree, by spatial uncertainty: statistical  
7 regularities give us a general sense as to where something useful might happen, and this  
8 evolves from moment to moment. We navigate this uncertainty by dynamically deploying  
9 spatial attention.

10 Covert spatial attention improves behavioral performance at attended locations  
11 at the cost of performance at unattended locations (Posner, 1980), leading to a common  
12 metaphor that spatial selective attention acts as a 'spotlight' or 'zoom lens' (Shaw and  
13 Shaw, 1977; Posner, 1980; Eriksen and St. James, 1986; Carrasco, 2011). This  
14 attentional 'spotlight' is characterized by a specific size and location and traverses the  
15 visual field based on behavioral demands (Eriksen and St. James, 1986; Castiello and  
16 Umiltà, 1990), selectively boosting information at the attended location within the visual  
17 system while suppressing information elsewhere. Animal studies have observed  
18 multiplicative increases in visuocortical neural responses at attended locations  
19 (McAdams and Maunsell, 1999; Maunsell, 2015) and human neuroimaging studies have  
20 found similar focal modulations of population responses (Kastner *et al.*, 1998;  
21 Brefczynski and DeYoe, 1999; McMains and Somers, 2004; Datta and DeYoe, 2009;  
22 Sprague and Serences, 2013; Puckett and DeYoe, 2015; Samaha, Sprague and Postle,  
23 2016; Shioiri *et al.*, 2016; Bloem and Ling, 2019; Bartsch *et al.*, 2023).

24 While neural modulation at the locus of attention has been relatively well studied,  
25 less is known regarding the neural signatures of the size of the attentional field  
26 (Yeshurun, 2019). Spreading attention over a larger region of visual space can decrease  
27 behavioral performance, but only a handful of studies have interrogated associated  
28 effects within visual cortex (Müller *et al.*, 2003; Herrmann *et al.*, 2010; Itthipuripat *et al.*,  
29 2014; Feldmann-Wüstefeld and Awh, 2020). This is surprising, as the spatial distribution  
30 of the attentional field is a key feature in an influential theoretical model of attention  
31 (Reynolds and Heeger, 2009). The model assumes that the size of the attentional field  
32 can be adjusted based on task demands and that the interaction between attentional  
33 field size and stimulus-related factors can predict observed attentional gain effects.

34 While the studies that have experimentally manipulated the attentional field size  
35 found evidence congruent with this prominent theory (Herrmann *et al.*, 2010; Itthipuripat  
36 *et al.*, 2014; Kınıklıoğlu and Boyaci, 2022), few studies have directly investigated the  
37 spatial extent of the attentional window and its concomitant neural representation. One  
38 neuroimaging study revealed that the attentional field expanded in the face of greater  
39 task-related uncertainty (Herrmann *et al.*, 2010), while other studies showed that the  
40 responsive area of visual cortex increased in size, coupled with a decrease of the overall  
41 population response (Müller *et al.*, 2003; Feldmann-Wüstefeld and Awh, 2020). While  
42 these studies are consistent with the notion that the attentional field size can be detected

43 in visual cortex, methods for dynamically recovering location and field size from moment  
44 to moment are lacking.

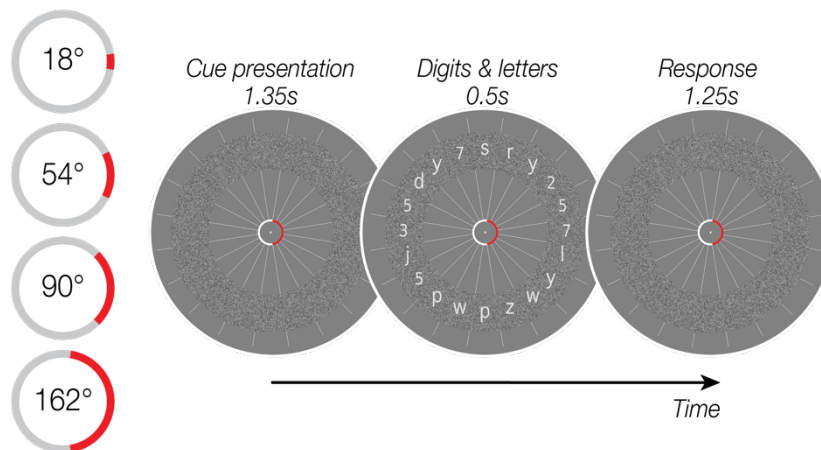
45 In this study, we developed a paradigm that allowed us to dynamically  
46 characterize the spatial tuning of spatial attention across the visual field. Using fMRI in  
47 humans, we examined whether attentional modulation of the BOLD response spanned  
48 a larger area of visual cortex when participants were cued to perform attend to a larger  
49 region of space. Behavioral performance confirmed that participants could successfully  
50 allocate their attention to different-sized swaths of the visual field. This deployment of  
51 attention was associated with a modulation in cortical activity in the corresponding  
52 retinotopic areas of visual cortex. By modeling the location and spread of the  
53 visuocortical modulation, we dynamically recovered the cued location from the  
54 attentional activity with a high degree of fidelity, together with a broadening of the  
55 attentional modulation for wider attentional cues.

# 1 Results

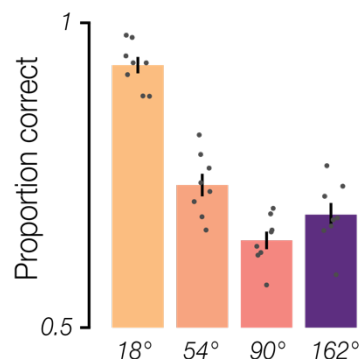
## 2 Behavioral performance indicates effective deployment of covert spatial attention

3 We set out to investigate the spatial distribution of attentional modulation within  
4 visual cortex. To do so, we first ensured that participants ( $n=8$ ) could successfully  
5 allocate covert spatial attention to cued portions of the visual field. During the  
6 experiment, participants' task was to fixate the center of the screen and report whether  
7 there were more *numbers* or *letters* in a cued peripheral region (**Figure 1a**). The cued  
8 region varied in location and width: it could be centered on any of 20 polar angles and  
9 could span any of four widths ( $18^\circ$ ,  $54^\circ$ ,  $90^\circ$ , and  $162^\circ$  of polar angle). Task performance  
10 indicated that participants used the cue effectively, as the proportion of correct  
11 responses was significantly above chance for all width conditions (**Figure 1b**; t-test, all  
12  $p < .001$ ). We verified, with eye tracking, that participants performed the task using  
13 peripheral vision while maintaining central fixation. The upper bound of the 95% CI for  
14 each participant's average gaze eccentricity ranged from  $0.29^\circ$  (degrees of visual angle)  
15 to  $0.64^\circ$  (mean =  $0.48^\circ$ ; **Figure 1c**), suggesting that gaze did not exceed the cue annulus  
16 at fixation and that participants used covert spatial attention to perform the task.

a. Attention task trial sequence



b. Behavioral task performance



c. Gaze distance from fixation

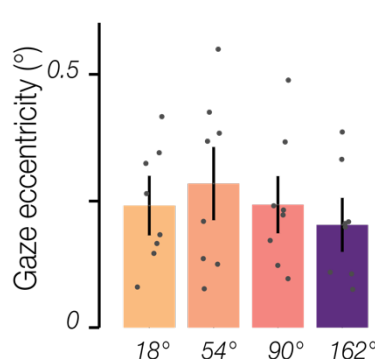


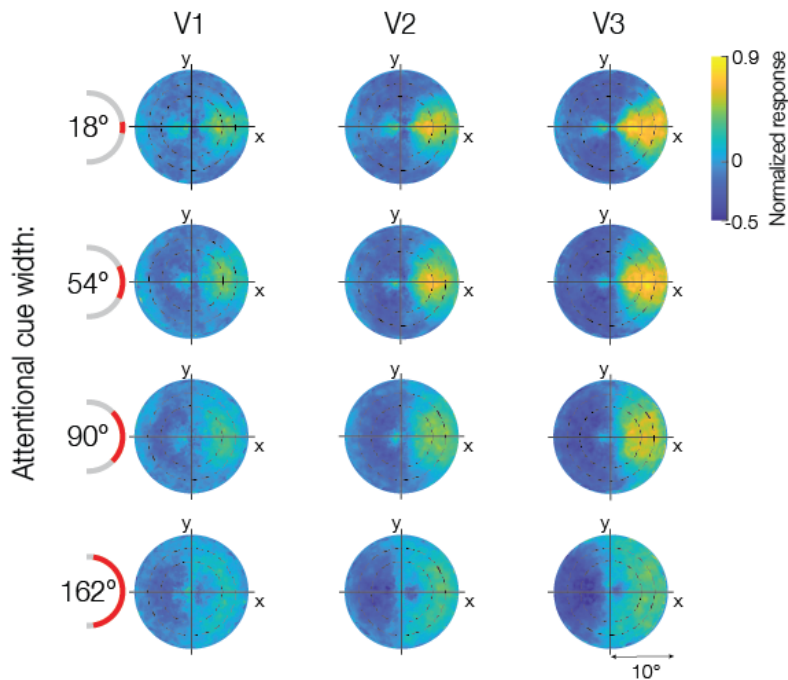
**Figure 1.** a. Task schematic. Participants were instructed to maintain central fixation and use covert spatial attention to determine whether there were more numbers or letters present within a cued region of a white noise annulus. On each trial, the red cue was displayed alone for 1.35 s and remained present throughout the trial. Twenty digits and letters were then presented for 0.5 s, equally spaced and overlaid on the annulus. Participants had 1.25 s to indicate via button press whether more digits or letters were present in the cued region. The cue remained stable for 5 trials (10 TRs, 15.5 s), had a width of 1, 3, 5, or 9 segments ( $18^\circ$ ,  $54^\circ$ ,  $90^\circ$ , or  $162^\circ$ ), and was centered on any of the 20 digit/letter slots. b. Behavioral task performance: Group mean accuracy for each cue width. Error bars are SEM; gray circles show individual participants. c. Group mean gaze eccentricity (in degrees of visual angle) for each cue width, conventions as in b.

17 **Attentional modulation of BOLD responses broadens with cue width**

18 We assessed the spatial distribution of attention by visualizing how the BOLD  
19 response was modulated by the location and width of the cue. To do so, we used each  
20 voxel's population receptive field (pRF) to project BOLD responses for each attentional  
21 cue into the visual field. The resulting 2D visual field maps were averaged across trials  
22 for each cue width by rotating the maps, so the attentional cue aligned to 0° polar angle  
23 (right horizontal meridian). The reconstructed visual field maps revealed that increasing  
24 cue width led to a concomitant broadening of attentional modulation in cortex (**Figure**  
25 **2a**). While this pattern was evident in all three early visual regions (V1–V3), the effect  
26 appeared to strengthen when ascending the visuocortical hierarchy.

27 Next, we computed the one-dimensional profile of attentional modulation at a  
28 fixed eccentricity. We were able to do this because we manipulated the location of the  
29 attentional field only as a function of polar angle, so all cues directed the attentional field  
30 to iso-eccentric locations. We selected voxels with pRFs that overlapped the white noise  
31 annulus and sorted them according to their polar angle preference.

a. Attention: 2D BOLD activity reconstruction



b. Spatial profile attentional modulation

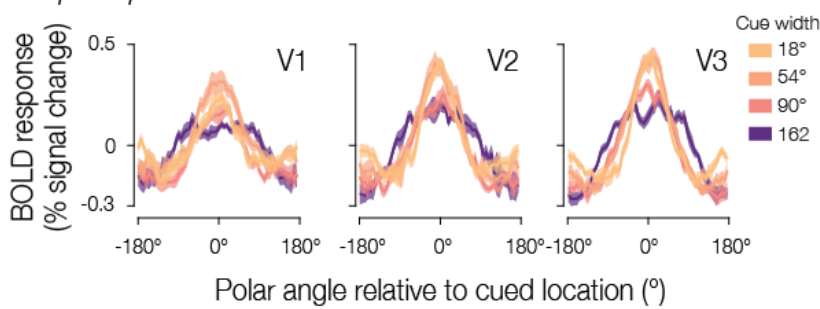


**Figure 2. a.** BOLD response projected into the visual field for each attentional cue width. Heatmaps represent the group mean BOLD activity using each voxel's population receptive field (pRF) location within the visual field, shown separately for V1, V2, and V3. Maps were rotated to align all attentional cue locations to 0° polar angle (rightward). Concentric circles indicated by black dashed lines represent the location of the white noise annulus. **b.** Average spatial modulation profiles at the eccentricity of the annulus. The spatial profiles were recentered to 0° polar angle based on the cue location. Solid lines represent the group mean BOLD response and shaded regions the SEM across participants.

32 For visualization purposes, the spatial response modulations were recentered to  
33 align all cues at 0° polar angle and averaged across trials for each cue width separately.  
34 Much like in the visual field reconstructions, there was a clear attentional modulation  
35 centered on 0°, which broadened and shifted downwards with cue width – a pattern that  
36 was particularly evident in area V3 (Figure 2b).

37 **Dynamic model-based recovery of the attentional field**

38 We next applied a modeling approach to estimate the location and width of  
39 attentional modulation, allowing us to further investigate the spread of attention in visual  
40 cortex. To do this, we averaged the spatial response profiles across TRs within each 10-  
41 TR block, in which the cue maintained a consistent location and width, yielding between  
42 27 and 53 averaged spatial response profiles per participant for each width condition.  
43 We fit a generalized Gaussian function to each of these spatial profiles to estimate the  
44 location and width of attentional modulation per spatial profile (see Figure 3a). The width  
45 of attentional modulation was quantified in terms of the full width at half maximum  
46 (FWHM) of the best fitting model prediction (see Figure 3b).

*a. Generalized Gaussian model b. Quantify attentional field*

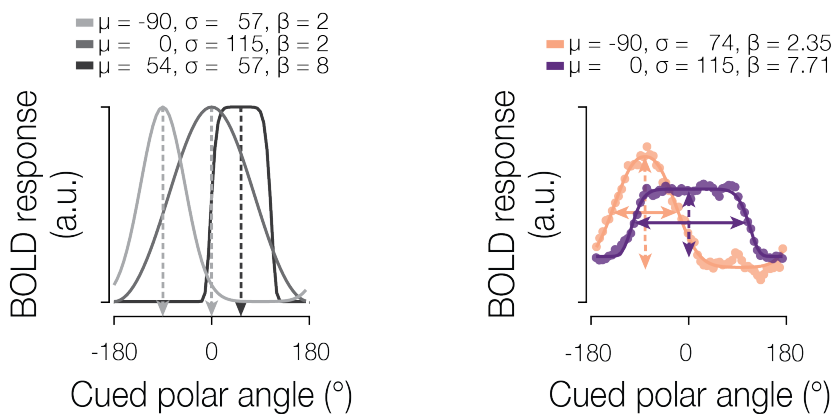


**Figure 3. a.** Modeling approach. The generalized Gaussian model is characterized by parameters for location ( $\mu$ ), scale ( $\sigma$ ), and shape ( $\beta$ ). **b.** Example model fits for two spatial profiles. Dots indicate BOLD response for two attentional cues differing in position and width. Solid lines indicate the best fitting model estimate. To quantify the attentional field, we extracted the location and gain (dashed arrows), as well as the width (FWHM; solid arrows).

47 Can we dynamically recover the attentional field from activity within visual cortex?  
48 Model fits explained a substantial proportion of variance in the spatial profiles of BOLD  
49 activity (**V1**: for 18° cues, mean [standard deviation] of  $R^2 = 0.42 [0.03]$ ; for 54° cues, 0.43  
50 [0.03]; for 90° cues, 0.44 [0.03]; for 162° cues, 0.42 [0.03]; **V2**: for 18° cues, 0.51 [0.05];  
51 for 54° cues, 0.54 [0.05]; for 90° cues, 0.54 [0.04]; for 162° cues, 0.55 [0.04]; **V3**: for 18°  
52 cues, 0.50 [0.03]; for 54° cues, 0.56 [0.04]; for 90° cues, 0.55 [0.03]; for 162° cues, 0.51  
53 [0.02]). To interpret the estimated model parameters, we excluded the bottom 20% of  
54 fits based on a pooled  $R^2$  across V1, V2, and V3, leaving roughly equal proportions of  
55 included blocks across cue width conditions (18°: mean [standard deviation] = 0.78  
56 [0.04], 54°: 0.83 [0.05], 90°: 0.83 [0.04], 162°: 0.77 [0.07]).

57 To assess how well the model-estimated attentional field matched the cued  
58 location, we first calculated the angular error between the cue center and the model's  
59 estimated location parameter. The angular error distribution across blocks, separated by  
60 width condition, is shown in **Figure 4** for one example participant to display block-to-  
61 block variation. The model reliably captured the location of the attentional field with low  
62 angular error and with no systematic directional bias. This result was observed across  
63 participants. We next examined the absolute angular error to assess the overall accuracy  
64 of our estimates. The group mean absolute angular error in V1 was  $41.9^\circ$  (SEM=2.86°),  
65 in V2 was  $32.2^\circ$  (2.31°), and in V3 was  $24.7^\circ$  (1.54°). Additionally, the magnitude of the  
66 absolute error did not vary linearly with the width of the cue in V1 or V2 (regression slopes  
67 tested against zero at the group level using a t-test; V1:  $t(7)=0.65$ ,  $p=.537$ ; V2:  $t(7)=1.24$ ,  
68  $p=.253$ ; **Figure 5**). In V3, we observed a small but statistically significant increase in  
69 absolute error magnitude associated with greater cue widths (mean slope=1.4,  $t(7)=4.18$ ,  
70  $p=.004$ ).

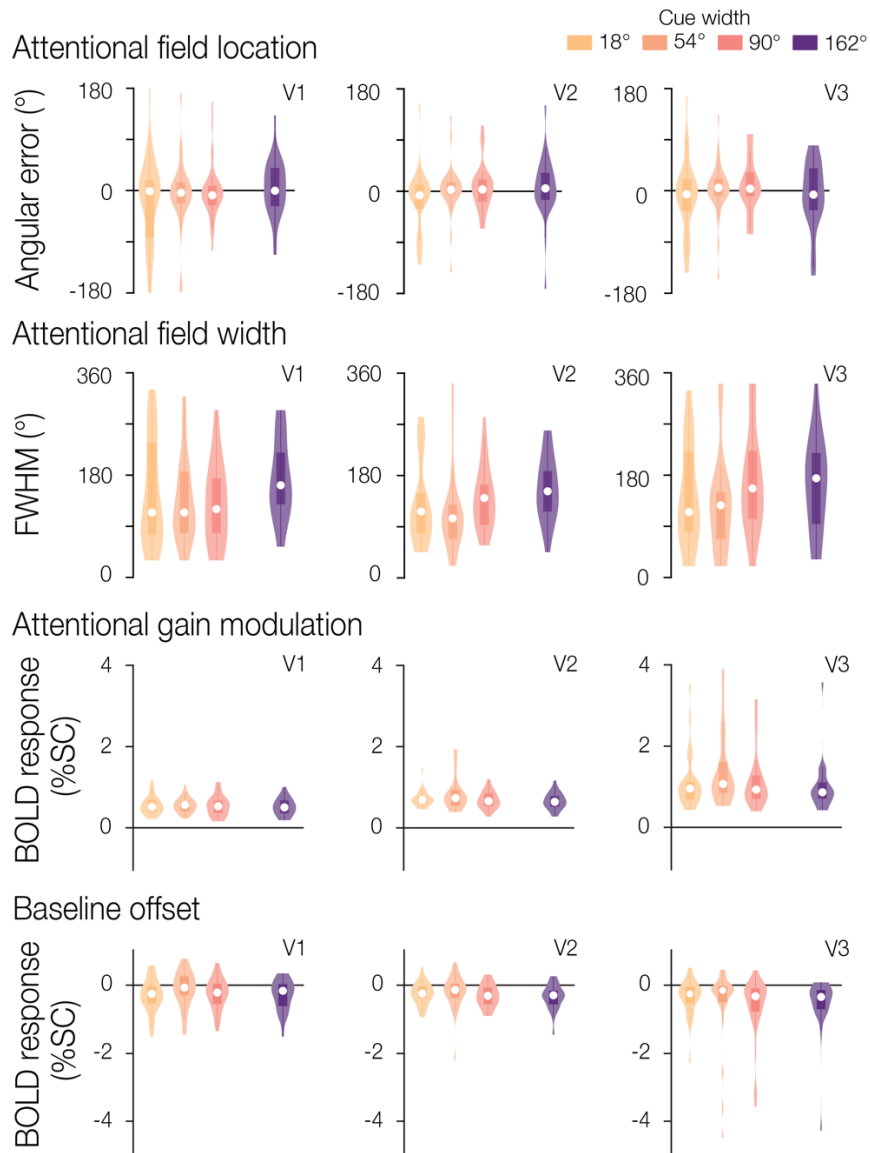
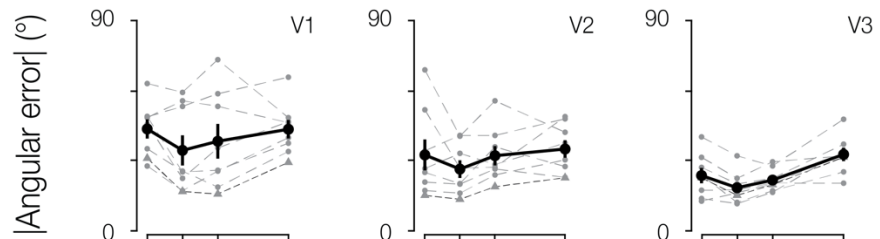


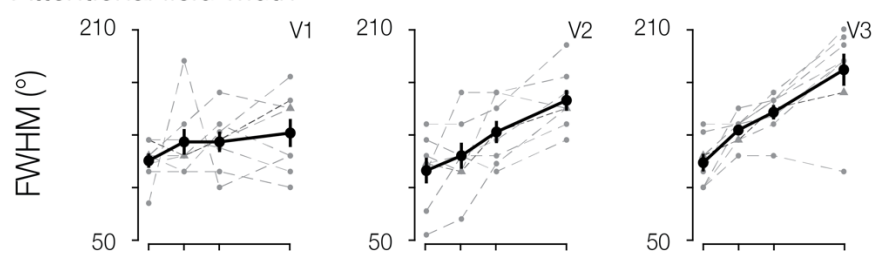
**Figure 4.** Attentional field parameter estimates for an example participant. The full parameter estimate distributions across blocks for location, width, gain, and baseline are shown for one example participant in V1, V2, and V3. Median parameter estimates are shown by the white points, with the box plot representing the 25th to 75th percentile, and whiskers extending to all non-outlier points.

71 Next, we evaluated the width of the attentional field by visualizing the distribution  
72 of FWHM for the same example participant (**Figure 4**), and at the group level (**Figure 5**).  
73 Confirming the broadening of the attentional field observed in the visual field  
74 reconstruction maps, we found that the estimated FWHM increased with greater cue

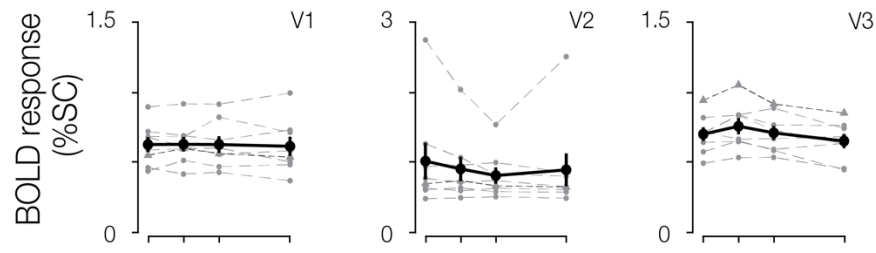
#### Attentional field location



#### Attentional field width



#### Attentional gain modulation



#### Baseline offset

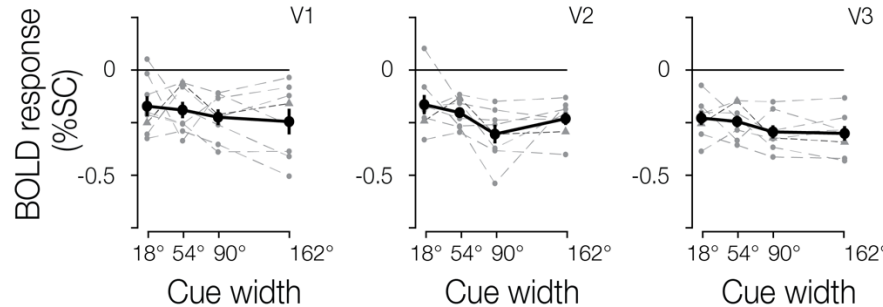


**Figure 5.** Attentional field parameter estimates. Group results for location, width, gain, and baseline estimates. Overall group mean and standard error are shown in solid black, separated by cue width and brain region. Individual participant median estimates are shown in grey. The example participant from Figure 4 is indicated by a denser dashed dark gray line with triangle symbols to aid in comparison.

75 widths in V2 and V3 (V2  $t(7)=5.63, p<.001$ ; V3  $t(7)=6.49, p<.001$ ). The effect was not  
76 statistically significant in V1 ( $t(7)=1.68, p=.136$ ).

77 We also assessed the gain of the attentional modulation in the model (**Figure 4**  
78 and **5** for the example participant and group data, respectively). We observed no  
79 significant relationship between gain and cue width in V1 and V2 (V1  $t(7)=-.54, p=.605$ ;  
80 V2  $t(7)=-2.19, p=.065$ ), though we did find a significant effect in V3 illustrating that gain  
81 decreases with cue width ( $t(7)=-3.12, p=.017$ ). We also found that the overall gain was  
82 greater in V2 and V3 compared to V1 (paired t-test, both  $p<=.01$ ).

83 Finally, we examined the baseline offset (**Figure 4** example participant, and  
84 **Figure 5** group data). No significant relationship was observed between cue width and  
85 baseline offset in any of the three brain regions (V1,  $t(7)=-1.05$ ,  $p=.330$ ; V2,  $t(7)=-2.00$ ,  
86  $p=.086$ ; V3,  $t(7)=-1.61$ ,  $p=.152$ ).

87 **Temporal interval analysis**

88 In the previous analyses, we leveraged the fact that the attentional cue remained  
89 constant for 5-trial blocks (spatial profiles were computed by averaging BOLD  
90 measurements across a block of 10 TRs). We next examined the degree to which we  
91 were able to recover the attentional field on a moment-by-moment (TR-by-TR) basis. To  
92 do this, we systematically adjusted the number of TRs that contributed to the averaged  
93 spatial response profile. To maintain a constant number of observations across the  
94 temporal interval conditions, we randomly sampled a subset of TRs from each block.  
95 This allowed us to determine the amount of data needed to recover the attentional field,  
96 with a goal of examining the usability of our modeling approach in future paradigms  
97 involving more dynamic deployment of spatial attention.

98 When we systematically varied the number of TRs included for each model fit (1,  
99 2, 3, 5, or 10 TRs), we found a significant effect of cue width on recovered FWHM when  
100 averaging two or more TRs in V3 (all  $t(7)>=2.38$ , all  $p<=.049$ ), and ten TRs in V2 (results  
101 as reported in prior section; **Figure 6a**). As described above, V1 did not reliably show a  
102 significant relationship between cue width and FWHM, even when averaging ten TRs.  
103 We found that increasing the number of TRs had a small but significant positive effect  
104 on FWHM estimates in V2 and V3 (V2, mean slope=2.7,  $t(7)=2.95$ ,  $p=.021$ ; V3, mean  
105 slope=1.16,  $t(7)=3.22$ ,  $p=.015$ ), although a significant effect was not observed in V1  
106 ( $t(7)=1.82$ ,  $p=.111$ ).

107 The number of TRs significantly affected the absolute angular error associated  
108 with the estimated location of the attentional field (**Figure 6b**). Error magnitude  
109 decreased with TRs in all three visual regions (all  $t(7)<=-4.48$ , all  $p<=.003$ ), suggesting  
110 that more data yielded more accurate estimates, though absolute angular error remained  
111 consistently below chance (90°) even when fitting the model to single-TR BOLD  
112 responses. Angular error remained stable across width conditions in V1 and V2 (V1,  $t(7)=-$   
113 .55,  $p=.598$ ; V2,  $t(7)=1.92$ ,  $p=.098$ ), though we found that larger cue width had a small  
114 but significant effect associated with larger errors in V3 (mean slope=.02,  $t(7)=3.28$ ,  
115  $p=.014$ ).

116 The estimated gain of the attentional modulation showed a dependence on  
117 number of TRs, with more TRs associated with lower gain estimates in V1 and V3 (V1,  
118  $t(7)=-7.21$ ,  $p<.001$ ; V3,  $t(7)=-9.97$ ,  $p<.001$ ), though this was not clearly observed in V2  
119 ( $t(7)=-1.60$ ,  $p=.154$ ). There was no evident dependence of gain on cue width in V1 and  
120 V2 (V1  $t(7)=-.19$ ,  $p=.856$ ; V2  $t(7)=-2.34$ ,  $p=.052$ ), though we did observe a significant  
121 relationship in V3 ( $t(7)=-2.86$ ,  $p=.024$ ; **Figure 6c**).

122 The baseline offset tended to increase with number of TRs across all three brain  
123 regions (V1,  $t(7)=8.79$ ,  $p<.001$ ; V2,  $t(7)=6.5$ ,  $p<.001$ ; V3,  $t(7)=5.59$ ,  $p=.001$ ; **Figure 6d**).  
124 Baseline offset did not show a significant dependence on cue width in any region (V1,  
125  $t(7)=1.47$ ,  $p=.186$ ; V2,  $t(7)=-2.16$ ,  $p=.068$ ; V3,  $t(7)=-1.67$ ,  $p=.139$ ).

126 Finally, the model's goodness of fit improved with more data, with larger  $R^2$   
127 associated with greater numbers of TRs included in the average profiles (all  $t(7) \geq 2.99$ ,  
128 all  $p \leq 0.020$ ), though all  $R^2$  were above 0.3 across all visual regions even for single-TR  
129 model fits. We did not observe a dependence of  $R^2$  on cue width (all  $t(7) \leq 1.26$ , all  
130  $p \geq .249$ ; **Figure 6e**).

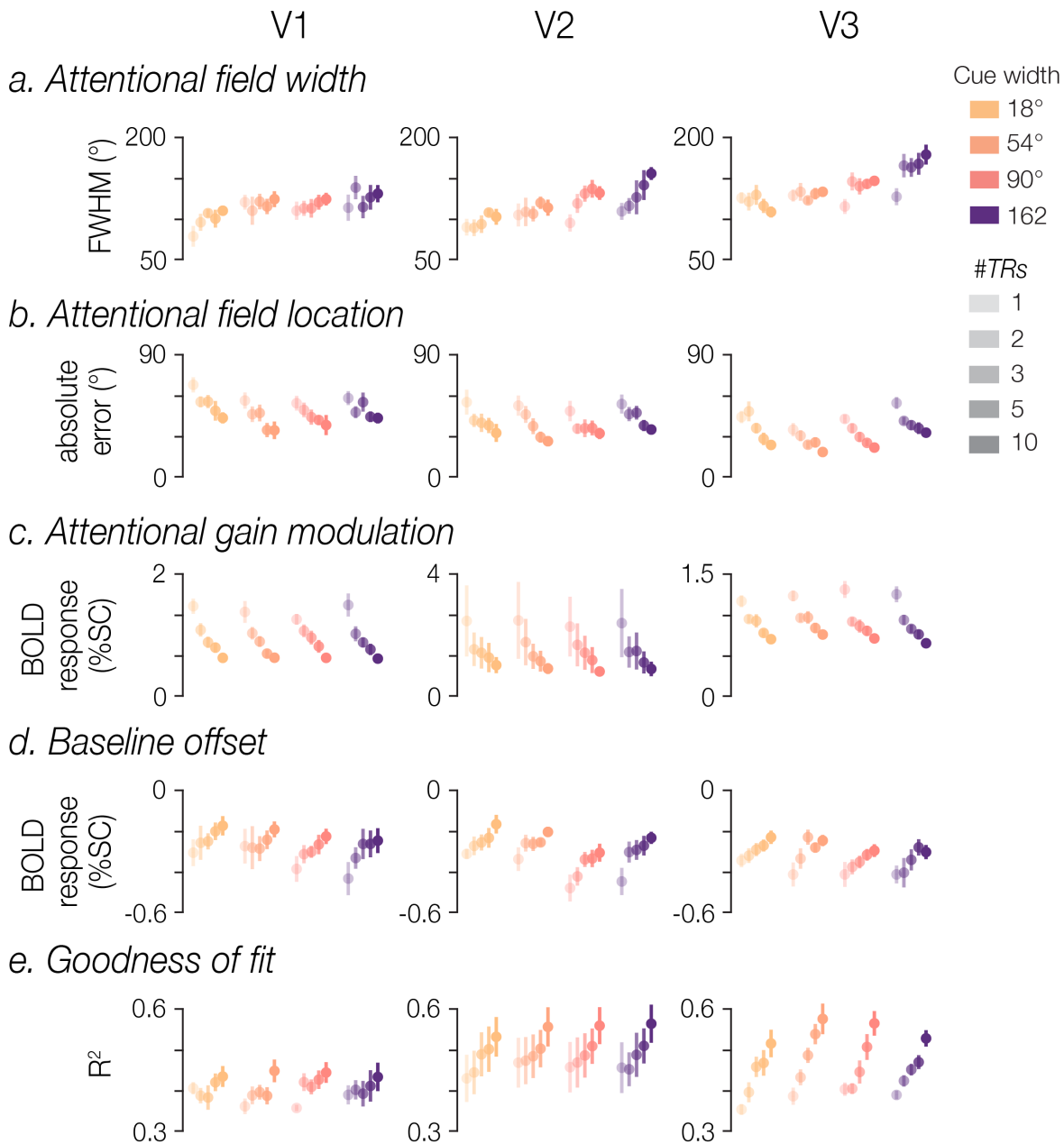


**Figure 6.** Effect of number of TRs. Model fits were computed using BOLD data averaged across different temporal intervals (1, 2, 3, 5, or 10 TRs). Group means (with SEM) are plotted for FWHM, absolute angular error, gain, baseline estimates, and  $R^2$ , separated by cue width, brain region, and the number of TRs used for each model fit.

131 **Width of the attentional field mimics perceptual modulation**

132 While the attentional field broadened as expected when participants were cued  
133 to attend to a larger portion of the white noise annulus, the size of the estimated  
134 attentional modulation was greater than the true size of the cued region. The cue width  
135 varied between 18° and 162°, whereas the width estimate derived from spatial profiles  
136 of BOLD modulation varied between 103° and 179° (**Figure 5**). We wondered what the  
137 underlying cause of this disparity might be. One possibility is that the BOLD-derived  
138 FWHM might tend to overestimate the retinotopic extent of the modulation, perhaps  
139 driven by binning and smoothing processing steps to create the 1D spatial profiles. If  
140 this were the case, we would expect to obtain similar FWHM estimates when modeling  
141 the perceptual modulations as well. Alternatively, the true subjective attentional field  
142 might be consistently broader than cued, despite the presence of nearby distractors. If  
143 this were the case, modulation driven by perceptual differences should *not* result in the  
144 same large FWHM estimates.

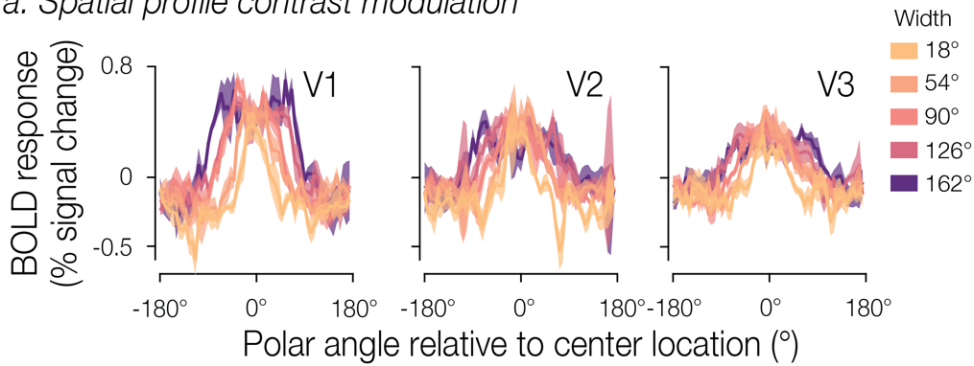
145 To address this, we compared our estimates of the attentional field with  
146 equivalent estimates for spatial profiles induced by a perceptual manipulation. In this  
147 additional experiment, we varied the contrast intensity of sections of the white noise  
148 annulus. Participants were not asked to deploy spatial attention to the stimulus and were  
149 instead instructed to perform a color change detection task at fixation. The regions of  
150 increased noise contrast matched the attentional cue widths (18°, 54°, 90°, and 162°,  
151 plus an additional intermediate width of 126°), and were centered on one of the four  
152 cardinal locations (0°, 90°, 180°, 270° polar angle).

153 As expected, we observed a broadening of the spatial profile of BOLD modulation  
154 in all three visual areas as the region of increased contrast widened (**Figure 7a**). Using  
155 an identical modeling procedure, we estimated the spatial profile of the *perceptual* BOLD  
156 modulation. The model-based estimates revealed that the mean magnitude of angular  
157 error between the model-estimated location and the center of the contrast stimulus had  
158 no significant dependence on contrast width in any of the three brain regions (magnitude  
159 of all  $t(4) \leq .915$ , all  $p \geq .412$ ). The recovered FWHM increased with contrast width in  
160 both V1 and V3 (**Figure 7b**; V1,  $t(4)=6.94$ ,  $p=.002$ ; V3  $t(4)=11.34$ ,  $p<.001$ ), though this  
161 effect was not clearly observed in V2 ( $t(4)=1.37$ ,  $p=.242$ ). The estimated gain modulation  
162 also did not show a relationship to contrast width in any of the visual areas (magnitude  
163 of all  $t(4) \leq 1.71$ , all  $p \geq 0.163$ ). Finally, we did not observe a significant relationship  
164 between contrast width and baseline offset in any visual area (magnitude of all  
165  $t(4) \leq 1.93$ , all  $p \geq 0.125$ ). In sum, the group results for model estimates revealed that: 1)  
166 the model was highly accurate in estimating the location of the contrast increment; 2)  
167 FWHM of the spatial profiles broadened across contrast widths, 3) the gain and baseline  
168 remained stable across contrast widths (**Figure 7b**).

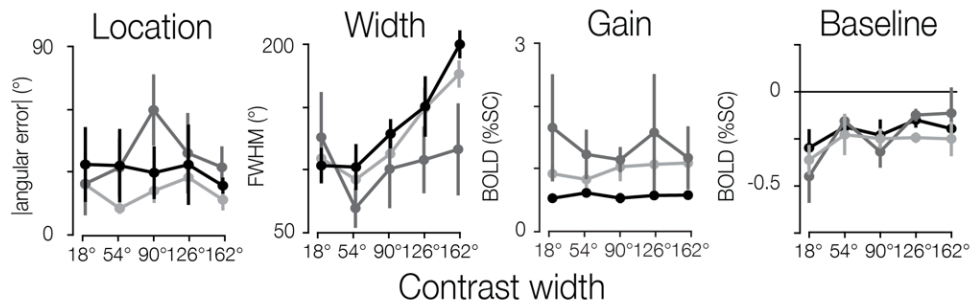
169 Mirroring the results from the attentional manipulation, FWHM estimates  
170 systematically exceeded the nominal size of the perceptually modulated region of the  
171 visual field. Comparing the estimated FWHMs of the perceptual and attentional spatial  
172 profiles (**Figure 7c**) revealed that the estimated widths were highly comparable (Pearson  
173 correlation  $r=0.664$  across width conditions and visual regions). Importantly, the relative

174 differences in FWHM show meaningful effects of both cue and contrast width in a similar  
175 manner for attentional and perceptual forms of modulation.  
176

*a. Spatial profile contrast modulation*



*b. Group results*



*c. FWHM comparison*

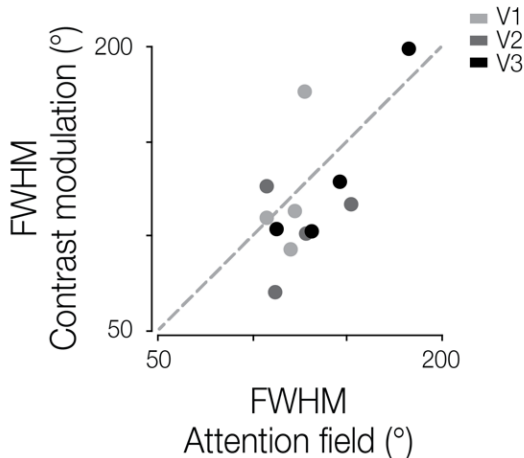


**Figure 7. a.** Spatial profiles of perceptual modulation. Solid lines represent the group mean BOLD activity and shaded regions the SEM. **b.** Group level parameter estimates. Overall group mean and standard error are shown for the absolute angular error, FWHM, gain and baseline, separated by contrast width and brain region. **c.** Comparison of FWHM estimates obtained from the attentional manipulation and the physical contrast manipulation. Dot color indicates brain region; each point represents the mean FWHM for a given width condition across participants.

## 1 Discussion

2 We investigated the topographic spread of spatial attention in human visual cortex  
3 by characterizing the spatial profile of BOLD responses while participants attended to  
4 different portions of the visual field. Behavioral performance confirmed that participants  
5 used the fixation cue to dynamically allocate attention to different swaths of the visual  
6 field. Attention allocation was associated with a modulation in the BOLD response in  
7 corresponding retinotopic areas of visual cortex. To characterize the topography of that  
8 modulation, our approach involved selecting voxels with pRF preferred eccentricities  
9 that overlapped our white noise annulus, and organizing those voxels into one-  
10 dimensional profiles of attentional modulation as a function of preferred polar angle. This  
11 allowed us to model the location and spread of the attentional field and test how well it  
12 tracked the nominal location and width of the cue presented at fixation. Using a  
13 generalized Gaussian model, the cued location could be recovered with high fidelity. We  
14 observed a broadening of the estimated attentional field in areas V2 and V3 with the cue  
15 width, suggesting our method was capable of dynamically recovering the location and  
16 size of the attentional field from moment to moment. We also found that the estimated  
17 spatial spread of the attentional modulation (as indicated by the recovered FWHM) was  
18 consistently wider than the cued region itself. We therefore compared the spread of the  
19 attention field with the spatial profile of a *perceptually* induced width manipulation. The  
20 results were comparable in both the attentional and perceptual versions of the task,  
21 suggesting that cueing attention to a region results in a similar 1D spatial profile to when  
22 the stimulus contrast is simply increased in that region.

23 This work builds on the concept of an attentional ‘spotlight’ or ‘zoom lens’ that has  
24 long been theorized to aid in spatial attention (Shaw and Shaw, 1977; Posner, 1980;  
25 Eriksen and St. James, 1986; Carrasco, 2011). By flexibly adjusting and shifting the focus  
26 of the spotlight, visual representations are selectively enhanced in a region of the visual  
27 field. However, the empirical evidence demonstrating that attention can change its  
28 spread across the visual field by modulating brain responses is surprisingly lacking  
29 (Yeshurun, 2019). Our understanding of how the attentional window interacts with spatial  
30 representations is mainly based on behavioral reports (Gobell, Tseng and Sperling, 2004;  
31 Palmer and Moore, 2009; Herrmann *et al.*, 2010; Beilen *et al.*, 2011; Taylor *et al.*, 2015;  
32 Huang *et al.*, 2017; Kınıklıoğlu and Boyaci, 2022), but see (Müller *et al.*, 2003; Hopf *et al.*,  
33 2006; Itthipuripat *et al.*, 2014; Tkacz-Domb and Yeshurun, 2018; Feldmann-Wüstefeld  
34 and Awh, 2020). We introduced a novel modeling approach that recovered the location  
35 and the size of the attentional field. Our data show that the estimated spatial spread of  
36 attentional modulation (as indicated by the recovered FWHM) consistently broadened  
37 with the cue width, replicating prior work (Müller *et al.*, 2003; Herrmann *et al.*, 2010). Our  
38 results go beyond prior work by linking the spatial profiles to pRF estimates, allowing us  
39 to quantify the spread of both attentional and perceptual modulation in degrees of polar  
40 angle. Interestingly, the FWHM estimates for the attentional and perceptual spatial  
41 profiles were highly similar. Additionally, for area V3 we replicate that the population  
42 response magnitude decreased with cue width (Müller *et al.*, 2003; Feldmann-Wüstefeld

43 and Awh, 2020). One innovation of our method is that it directly reconstructs attention-  
44 driven modulations of responses in visual cortex, setting it apart from other methods,  
45 such as inverted encoding models (e.g. Sprague and Serences, 2013). Finally, we  
46 demonstrated that our method has potential to be used in more dynamic settings, in  
47 which changes in the attentional field need to be tracked on a shorter timescale.

48 The ability to change the size of the attentional field is a crucial component in an  
49 influential theoretical model of attention. This model proposes that the interaction  
50 between stimulus properties (such as its size and specific features) and the attentional  
51 field can explain a wide variety of attentional effects reported in behavioral and  
52 neurophysiological studies (Herrmann *et al.*, 2010; Itthipuripat *et al.*, 2014; Bloem and  
53 Ling, 2019; Jigo, Heeger and Carrasco, 2021). The present study sought to address this  
54 gap, with our results showing that the visuocortical attentional field broadened as we  
55 increased the cue width (**Figure 5**). This provides compelling evidence that the attention-  
56 related cortical response can, in fact, flexibly vary in its position and spatial distribution.

57 The observed effects of attentional field width were unlikely to be directly  
58 attributable to variation in task difficulty. Participants' task in our study was to  
59 discriminate whether more numbers or more letters were presented within a cued region  
60 of an iso-eccentric annulus of white noise. For our different cue widths, the ratios of  
61 numbers and letters were selected to be as similar as possible given the size and spacing  
62 of our stimuli. Changes in accuracy across the three larger cue widths were small and  
63 non-monotonic, implying task difficulty was dissociable from width per se. This  
64 dissociation bolsters the interpretability of our model fits; nevertheless, future work  
65 should further investigate how task difficulty interacts with the spread of the attentional  
66 field and the amplitude of attention-related BOLD effects (cf. Ress, Backus and Heeger,  
67 2000).

68 In this study, we modeled the attentional field using a one-dimensional  
69 distribution. This approach aligned with our experimental design, as the attentional cue  
70 was manipulated only as a function of polar angle. However, we know that spatial  
71 processing varies substantially as a function of eccentricity. Spatial resolution is highest  
72 at the fovea and rapidly drops in the periphery (Anton-Erxleben and Carrasco, 2013). The  
73 spatial distribution of attention will presumably also vary with eccentricity and will likely  
74 take on different functional properties close to the fovea, where spatial resolution is high,  
75 compared to the far periphery where spatial resolution is low (Intriligator and Cavanagh,  
76 2001; Jigo, Heeger and Carrasco, 2021). Future work can help provide a better  
77 understanding of the contribution of spatial attention by considering how the attentional  
78 field interacts with these well described spatial variations across the visual field.  
79 Measuring the full spatial distribution of the attentional field (across both eccentricity and  
80 polar angle) will shed light on how spatial attention guides perception by interacting with  
81 the non-uniformity of spatial representations.

82 The spread of the attentional field likely influences the degree to which spatial  
83 resolution at the attended location is transformed, leading to enhanced behavioral  
84 performance. Spatial attention was vital for this task, as enhanced spatial perception  
85 allowed the participants to better discriminate all stimuli within the cued region (Anton-  
86 Erxleben and Carrasco, 2013). Future work could unpack the degree to which the size  
87 of the attentional field influences the spatial resolution of visual cortical representations

88 (Klein, Harvey and Dumoulin, 2014; Vo, Sprague and Serences, 2017; Tünçok, Carrasco  
89 and Winawer, 2024), and how this influences spatial perception.

90 Beyond addressing core questions related to the function of spatial attention, this  
91 method also lays groundwork for addressing questions about spatial predictive  
92 uncertainty and belief updating. Prior work on these topics has relied almost entirely on  
93 inferring participants' predictions from their behavior, often requiring participants to  
94 report overt point predictions (Nassar *et al.*, 2010; McGuire *et al.*, 2014; D'Acremont and  
95 Bossaerts, 2016; Nassar, Bruckner and Frank, 2019), or inferring participants'  
96 predictions from their sequences of decisions (Daw *et al.*, 2006; Behrens *et al.*, 2007;  
97 Payzan-LeNestour and Bossaerts, 2011; Payzan-LeNestour *et al.*, 2013). These  
98 approaches have shed light on how we dynamically adapt our learning and belief  
99 updating processes over time in differently structured contexts. However, methods for  
100 recovering information about full predictive belief distributions have been limited, relying  
101 on indirect measurements such as eye movements (O'Reilly *et al.*, 2013; Bakst and  
102 McGuire, 2021, 2023), and physiological measures of uncertainty and surprise in EEG  
103 and pupillometry (Preuschoff, 't Hart and Einhäuser, 2011; Nassar *et al.*, 2012; Nassar,  
104 Bruckner and Frank, 2019). The methods developed here offer a potential way to recover  
105 the location and width of a spatial predictive distribution via the attentional field in  
106 contexts in which it is unknown *a priori* and might be dependent on how a given  
107 participant has integrated previous sequential evidence. Future work could extend this  
108 method to more directly interrogate how predictive uncertainty is represented  
109 throughout the brain on a moment-by-moment basis.

110 In summary, we found evidence that people could dynamically adapt the spread  
111 of spatial attention, and that the retinotopic extent of attentional modulation of the BOLD  
112 response reflected this dynamic adaptation. These findings address a gap in our  
113 understanding of spatial attentional control, supporting core theoretical models of  
114 attention. Our modeling approach also lays the groundwork to address further questions  
115 related to how the attentional field interacts with the non-uniformity of spatial  
116 representations and how uncertainty in spatial contexts is represented in the human  
117 brain.

## 1 Materials and Methods

2 **Participants.** Eight healthy adults (4 female, 4 male, mean age = 30) participated in the  
3 main attention experiment, five of whom also participated in a second experiment  
4 featuring a contrast manipulation. All participants had normal or corrected-to-normal  
5 vision. All procedures were approved by the Boston University Institutional Review  
6 Board, and informed consent was obtained from all participants.

7  
8 **Apparatus and stimuli.** Participants were presented with stimuli generated using  
9 PsychoPy (v1.85.1; Peirce, 2007) on a MacBook Pro. The visual stimuli were displayed  
10 on a rear-projection screen (subtending  $\sim 20^\circ \times 16^\circ$  visual angle) using a VPixx  
11 Technologies PROPpixx DLP LED projector (maximum luminance 306 cd/m<sup>2</sup>).  
12 Participants viewed the screen through a front surface mirror. Participants were placed  
13 comfortably in the scanner with padding to minimize head motion.

14  
15 **Procedure.**  
16 *Attentional width manipulation.* Participants were instructed to fixate a central point  
17 (radius  $0.08^\circ$  visual angle) while dynamic pixelwise white noise (flickering at 10 Hz, 50%  
18 contrast) was presented in the periphery (annulus spanning  $4.6^\circ$  to  $7.4^\circ$  visual angle).  
19 The annulus was segmented into 20 bins ( $18^\circ$  polar angle per bin) by white grid lines  
20 radiating from a white circle at the center of the screen (radius  $0.25^\circ$ ), passing behind  
21 the annulus, and terminating at  $8.5^\circ$  eccentricity. In the middle of each bin, a number or  
22 letter (height:  $2.1^\circ$ ) was superimposed on the white noise annulus (see **Figure 1a**). For a  
23 subset of the participants (3 out of 8) the screen distance inside the scanner was  
24 changed, therefore for those participants the letter size was  $1.86^\circ$  visual angle, and the  
25 white noise annulus spanned  $4.1^\circ$  to  $6.5^\circ$  visual angle. The set of possible letters included  
26 all lowercase letters of the Latin alphabet except a, b, e, g, i, o, and u. The set of numbers  
27 included 2, 3, 4, 5, 7, and 8.

28 Participants were cued to attend covertly to a contiguous subset of the bins and  
29 their task was to report, via button press, whether there were more *numbers* or *letters*  
30 present within the cued region. The cue was a bold red segment on the central white  
31 circle, which corresponded to 1, 3, 5, or 9 bins ( $18^\circ$ ,  $54^\circ$ ,  $90^\circ$ , or  $162^\circ$  polar angle; see  
32 **Figure 1a**). The true proportion of letters versus numbers was controlled within each cue  
33 width condition. For cued regions of 1 bin, there was either a single number or letter in  
34 the bin. For cued regions of 3 bins, the ratio was always 2:1 (either two numbers and one  
35 letter or vice versa). For cued regions of 5 bins, the ratio was 3:2, and for cued regions  
36 of 9 bins, the ratio was 6:3. The ratios were selected to be as similar as possible given  
37 the size and spacing of our stimuli (aside from the one-bin cue, the proportions for the  
38 other cues were 0.67, 0.60 and 0.67). Cues could be centered on any of the 20 bins.

39 Participants completed 8 to 12 runs of the task (mean = 10.4), with each run  
40 lasting 341 s and containing 100 trials. Each cue remained constant for a block of five  
41 trials (lasting 15.5 s, 10 TRs), although the letters and numbers within the cued region  
42 changed on every trial. Thus, each participant saw 20 unique cues (combinations of cue

43 location and width) per run. Each run began and ended with 15.5 s of the dynamic noise  
44 annulus.

45 During each trial, the cue and white noise annulus were presented alone for 1.35  
46 s. The numbers and letters were then displayed for 0.5 s. Thereafter, the cue and white  
47 noise remained visible while the participant had 1.25 s to indicate whether there had  
48 been more digits or letters within the cued region, resulting in a total trial duration of 3.1  
49 s (2 TRs). No accuracy feedback was provided during the main experiment. However, all  
50 participants completed three training runs with trial-by-trial feedback prior to the scan  
51 session. During training runs, the response window was shortened to 1 s and the  
52 remaining 0.25 s presented feedback in the form of a change in color of the fixation point  
53 (blue for correct responses and orange for incorrect responses).

54

55 *Physical contrast manipulation.* A subset of participants (n=5) also participated in an  
56 experiment that enhanced the physical contrast intensity of the dynamic visual noise in  
57 segments of the annulus. This additional experiment was carried out during the same  
58 scan session and allowed for benchmarking the detectability of stimulus-evoked  
59 modulation in visual cortex using our analyses. The stimuli and trial structure were similar  
60 to the attentional manipulation. The task differed in the following ways: (1) the contrast  
61 of the white noise annulus was increased to 100% for segments of the annulus  
62 corresponding to 1, 3, 5, 7 or 9 bins (18°, 54°, 90°, 126°, or 162° polar angle), with a  
63 Gaussian rolloff ( $\sigma = 15^\circ$ ) that spanned 25% of the furthest included bins and 25% of the  
64 adjacent excluded bins; (2) the enhanced segments were always centered on the  
65 cardinal directions (0°, 90°, 180°, and 270° polar angle); (3) the contrast increase  
66 remained constant for 15.5 seconds (10 TRs); (4) participants performed a color change  
67 detection task at fixation. Each unique combination of 4 locations and 5 widths of the  
68 contrast enhancement was shown once per run, with the order randomized. To estimate  
69 a baseline response, each run started and ended with 15.5 seconds without contrast  
70 modulation. Participants completed two runs total, each lasting 341 seconds (220 TRs).

71 Throughout the *physical contrast* runs, participants were instructed to fixate on a  
72 central point (radius 0.08° visual angle) and to press a button when the fixation point  
73 switched color (alternating white and red). The fixation point remained a color for at least  
74 one second and then had a 10% probability of switching every 100 ms. No cue was  
75 presented associated with the regions of increased contrast. Additionally, no letters or  
76 numbers were superimposed on the white noise annulus.

77

78 *Population receptive field mapping.* Population receptive field (pRF) estimates were  
79 obtained for each participant in a separate scan session. We used the experimental  
80 procedure as described in the Human Connectome Project 7T Retinotopy dataset  
81 (Benson *et al.*, 2018). Stimuli were composed of a pink noise background with colorful  
82 objects and faces at various spatial scales, displayed on a mean luminance gray  
83 background. Stimuli were updated at a rate of 15 Hz while participants performed a color  
84 change detection task at fixation. Participants viewed two types of mapping stimuli: (1)  
85 contracting/expanding rings and rotating wedges; (2) moving bar stimuli (Dumoulin and  
86 Wandell, 2008; Kay *et al.*, 2013). A total of 4-6 scans (300 TRs) were collected for each  
87 participant (2-3 scans per stimulus type). In this session, the field of view was restricted

88 to the occipital cortex to maximize SNR, thereby limiting the brain regions for which we  
89 had pRF estimates to V1, V2, and V3.

90

91 ***MRI data acquisition.*** All MRI data were acquired at Boston University's Cognitive  
92 Neuroimaging Center (Boston, Massachusetts) on a research-dedicated Siemens  
93 Prisma 3T scanner using a 64-channel head coil. A scanning session lasted 2 hours.  
94 All functional neuroimaging data were acquired using a simultaneous multislice (SMS)  
95 gradient echo echoplanar acquisition protocol (Moeller *et al.*, 2010; Setsompop *et al.*,  
96 2012): 2 mm isotropic voxels; FoV = 212 x 212 mm; 72 axial slices; TR = 1.55 s; TE =  
97 35.60 ms; flip angle = 72°; multiband acceleration factor 4. We computed distortion field  
98 maps by using a spin echo echoplanar protocol with opposite y-axis phase encoding  
99 directions (2 mm isotropic voxels; FOV = 212 x 212 mm; TR = 8850 ms; TE = 70.80 ms;  
100 flip angle = 90°). During a separate scan session, we acquired a whole-brain anatomical  
101 scan using a T1-weighted multi-echo MPRAGE 3d sequence (1 mm isotropic; FoV = 256  
102 x 256 mm; 176 sagittal slices; TR = 2530 ms; TE = 1.69 ms; flip angle = 7°), and the pRF  
103 scans (occipital coverage only; right-left phase encoding; 2 mm isotropic voxels; FoV =  
104 136 x 136 mm; 36 slices; TR = 1 s; TE = 35.4 ms; flip angle = 64°; multiband acceleration  
105 factor 3).

106

### 107 ***MRI data analysis.***

108 *Structural data preprocessing.* Whole brain T1-weighted anatomical data were analyzed  
109 using the standard 'recon-all' pipeline provided by Freesurfer software (Freesurfer  
110 version 5.3, (Fischl, 2012)), generating cortical surface models, whole-brain  
111 segmentation, and cortical parcellations.

112

113 *Functional data preprocessing.* All analyses were performed in the native space for each  
114 participant. First, EPI distortion correction was applied to all fMRI BOLD time-series data  
115 using a reverse phase-encode method (Andersson, Skare and Ashburner, 2003)  
116 implemented in FSL (Smith *et al.*, 2004). All functional data were then preprocessed using  
117 FS-FAST (Fischl, 2012), including standard motion-correction procedures, Siemens slice  
118 timing correction, and boundary-based registration between anatomical and functional  
119 volumetric spaces (Greve and Fischl, 2009). To facilitate voxel-wise analysis, no  
120 volumetric smoothing was performed and across-run within-modality robust rigid  
121 registration was applied (Reuter, Rosas and Fischl, 2010), with the middle time-point of  
122 the first run serving as the target volume, and the middle time-point of each subsequent  
123 run used as a movable volume for alignment. Lastly, data were detrended (0.005 Hz  
124 high-pass filter) and converted to percent signal change for each voxel independently  
125 using custom code written in MATLAB (version 2020b).

126

127 *Population receptive field mapping and voxel selection.* The time series were analyzed  
128 using the analyzePRF toolbox in MATLAB, implementing a compressive spatial  
129 summation pRF model (Kay *et al.*, 2013). The results of the pRF analysis were used to  
130 manually draw boundaries between early visual regions (V1, V2, and V3), which served  
131 as our regions of interest (ROIs).

132 Within each ROI, pRF modeling results were used to constrain voxel selection  
133 used in the main experiment. We excluded voxels with a preferred eccentricity outside  
134 the bounds of the pRF stimulus ( $<0.7^\circ$  and  $>9.1^\circ$ ), with a pRF size smaller than  $0.01^\circ$ , or  
135 with poor spatial selectivity as indicated by the pRF model fit ( $R^2 < 10\%$ ). Following our  
136 2D visualizations (see below), we further constrained voxel selection by only including  
137 voxels whose pRF overlapped with the white noise annulus. We included all voxels with  
138 an estimated eccentricity within the annulus bounds, as well as voxels with an estimated  
139 pRF size that would overlap the annulus.

140

141 *2D visualizations of attentional modulation.* To visualize the topography of attentional  
142 modulation under different cue widths, we projected the average BOLD responses for a  
143 given block (10 TRs with a consistent cue location and width, shifted by 3 TRs [4.65 s]  
144 to compensate for the hemodynamic delay) into the visual field using each voxel's pRF  
145 location. This method is similar to that described in (Favila, Kuhl and Winawer, 2022).  
146 First, we computed the Cartesian (x,y) coordinates from the pRF eccentricity and polar  
147 angle estimates for each voxel. Then, within a given ROI, we interpolated the BOLD  
148 responses over (x,y) space to produce a full-field representation. Each representation  
149 was then z-scored to allow for comparison across blocks, cue conditions, and  
150 participants. Finally, the representation was rotated so that the center of the cue was  
151 aligned to the right horizontal meridian (see **Figure 2a**).

152

153 *1D spatial profile of attentional modulation.* We also examined the spatial profile of  
154 attentional modulation as a function of polar angle. Voxels with pRFs overlapping the  
155 white noise annulus were grouped into 60 bins according to their pRF polar angle  
156 estimate ( $6^\circ$  polar angle bin width). We computed a median BOLD response within each  
157 bin. This facilitated the recentering of each profile to align all cue centers for subsequent  
158 combining across trials. To improve the signal-to-noise ratio, the resulting profile was  
159 smoothed with a moving average filter (width  $18^\circ$  polar angle; see **Figure 2b**).

160

161 *Model fitting.* We quantified the spatial profile of attentional modulation with a  
162 generalized Gaussian model (Nadarajah, 2005). The generalized Gaussian function ( $G$ )  
163 combines Gaussian and Laplace distributions:

$$G = \exp \left\{ - \left| \frac{x - \mu}{\sigma} \right|^\beta \right\} \quad (1)$$

164 The function has free parameters for location ( $\mu$ ), scale ( $\sigma$ ), and shape ( $\beta$ ). The shape  
165 parameter enables the tails of the distribution to become heavier than Gaussian (when  
166  $\beta < 2$ ), or lighter than Gaussian (when  $\beta > 2$ ); as  $\beta \rightarrow \infty$ , the model approaches a  
167 uniform distribution.

168

169 Next,  $G$  was normalized to range between 0 and 1, and vertically scaled and shifted by  
170 two additional free parameters for gain ( $a$ ) and baseline offset ( $b$ ):

$$\hat{y} = a \cdot G + b \quad (2)$$

171 We fit the five free parameters ( $\mu, \sigma, \beta, a, b$ ) using the MATLAB optimization tool *fmincon*,  
172 minimizing the squared error between the model prediction and the 1D profile described  
173 above. To avoid local minima, we first ran a grid search to find the initialization values  
174 with the lowest SSE (6 possible values for  $\mu$ , equally spaced between 0 and 360°,  
175 crossed with 6 possible values for  $\sigma$ , equally spaced between 9° and 162° polar angle;  
176  $\beta = 4$ ;  $a = 1$ ;  $b = 0$ ). We imposed the following parameter bounds on the search:  $\sigma$ : [6°,  
177 180° polar angle],  $\beta$ : [1.8, 50], and  $a$ : [0, 20].  $\mu$  was unbounded, but was wrapped to  
178 remain within [0°, 360°].

179 From the model fits we computed the following summary metrics: 1) angular error,  
180 defined as the polar-angle distance between the true and estimated location; 2) the full  
181 width at half-maximum (FWHM) of the best-fitting generalized Gaussian function, which  
182 served as our measure of the width of attentional modulation. The FWHM was controlled  
183 mainly by the scale parameter ( $\sigma$ ) but also to a lesser degree by the shape parameter ( $\beta$ ;  
184 see **Figure 3a**); 3) the gain modulation of the spatial profile ( $a$ ); 4) the model's goodness  
185 of fit quantified as the percentage of explained variance ( $R^2$ ) in the spatial response  
186 profile:

$$R^2 = 1 - \frac{(y - \hat{y})^2}{(y - \bar{y})^2} \quad (3)$$

187 **Statistical testing.** To assess how the attentional cue width manipulation influenced the  
188 1D spatial profile of BOLD modulation, we tested whether the computed summary  
189 metrics (absolute angular error, FWHM, gain, and baseline) varied as a function of cue  
190 width. Specifically, we performed a linear regression for each metric within each subject  
191 and tested whether the slopes differed from zero at the group level using a t-test. This  
192 was done independently for each ROI. No multiple comparison correction was applied,  
193 as the different tests for each region are treated as separate questions. However, using  
194 a threshold of 0.017 for p-values would correct for comparisons across the three brain  
195 regions. When testing whether the number of TRs impacted our metrics, the linear  
196 regression used both cue width and number of TRs as explanatory variables.  
197

198 **Eye-position monitoring.** Gaze data were collected for all participants using an MR-  
199 compatible SR Research EyeLink 1000+ eye tracker sampling at 1 kHz. Data from blink  
200 periods were excluded from analysis. Participants maintained fixation throughout the  
201 task, with average gaze eccentricity below 0.5° for all participants. Gaze eccentricity did  
202 not significantly vary by cued width (pairwise comparison of width conditions using a  
203 paired t-test, all  $p \geq 0.205$  with Bonferroni correction for multiple comparisons) nor  
204 location (pairwise comparison, all  $p \geq 0.522$  with Bonferroni correction for multiple  
205 comparisons). Additionally, we examined the number of fixations to the white noise

206 annulus itself. No participant had more than 16 fixations (out of 800-1200 trials) to the  
207 annulus during the task, further suggesting that participants successfully maintained  
208 fixation.

## 1 References

- 2 1) Andersson, J.L.R., Skare, S. and Ashburner, J. (2003) 'How to correct susceptibility  
3 distortions in spin-echo echo-planar images: application to diffusion tensor imaging',  
4 *NeuroImage*, 20(2), pp. 870–888. Available at: [https://doi.org/10.1016/S1053-8119\(03\)00336-7](https://doi.org/10.1016/S1053-8119(03)00336-7).
- 6 2) Anton-Erxleben, K. and Carrasco, M. (2013) 'Attentional enhancement of spatial  
7 resolution: linking behavioural and neurophysiological evidence', *Nature Reviews  
8 Neuroscience*, 14(3), pp. 188–200. Available at: <https://doi.org/10.1038/nrn3443>.
- 9 3) Bakst, L. and McGuire, J.T. (2021) 'Eye movements reflect adaptive predictions and  
10 predictive precision', *Journal of Experimental Psychology: General*, 150(5), pp. 915–  
11 929. Available at: <https://doi.org/10.1037/xge0000977>.
- 12 4) Bakst, L. and McGuire, J.T. (2023) 'Experience-driven recalibration of learning from  
13 surprising events', *Cognition*, 232, p. 105343. Available at:  
14 <https://doi.org/10.1016/j.cognition.2022.105343>.
- 15 5) Bartsch, M.V. *et al.* (2023) 'A cortical zoom-in operation underlies covert shifts of  
16 visual spatial attention', *Science Advances*, 9(10), p. eade7996. Available at:  
17 <https://doi.org/10.1126/sciadv.ade7996>.
- 18 6) Behrens, T.E.J. *et al.* (2007) 'Learning the value of information in an uncertain world',  
19 *Nature Neuroscience*, 10(9), pp. 1214–1221. Available at:  
20 <https://doi.org/10.1038/nn1954>.
- 21 7) Beilen, M. van *et al.* (2011) 'Attentional Window Set by Expected Relevance of  
22 Environmental Signals', *PLOS ONE*, 6(6), p. e21262. Available at:  
23 <https://doi.org/10.1371/journal.pone.0021262>.
- 24 8) Benson, N.C. *et al.* (2018) 'The Human Connectome Project 7 Tesla retinotopy  
25 dataset: Description and population receptive field analysis', *Journal of Vision*, 18(13),  
26 p. 23. Available at: <https://doi.org/10.1167/18.13.23>.
- 27 9) Bloem, I.M. and Ling, S. (2019) 'Normalization governs attentional modulation within  
28 human visual cortex', *Nature Communications*, 10(1), p. 5660. Available at:  
29 <https://doi.org/10.1038/s41467-019-13597-1>.
- 30 10) Brefczynski, J.A. and DeYoe, E.A. (1999) 'A physiological correlate of the "spotlight"  
31 of visual attention', *Nature Neuroscience*, 2(4), pp. 370–374. Available at:  
32 <https://doi.org/10.1038/7280>.
- 33 11) Carrasco, M. (2011) 'Visual attention: The past 25 years', *Vision Research*, 51(13), pp.  
34 1484–1525. Available at: <https://doi.org/10.1016/j.visres.2011.04.012>.
- 35 12) Castiello, U. and Umiltà, C. (1990) 'Size of the attentional focus and efficiency of  
36 processing', *Acta Psychologica*, 73(3), pp. 195–209. Available at:  
37 [https://doi.org/10.1016/0001-6918\(90\)90022-8](https://doi.org/10.1016/0001-6918(90)90022-8).

38 13) D'Acremont, M. and Bossaerts, P. (2016) 'Neural Mechanisms Behind Identification  
39 of Leptokurtic Noise and Adaptive Behavioral Response', *Cerebral Cortex*, 26(4), pp.  
40 1818–1830. Available at: <https://doi.org/10.1093/cercor/bhw013>.

41 14) Datta, R. and DeYoe, E.A. (2009) 'I know where you are secretly attending! The  
42 topography of human visual attention revealed with fMRI', *Vision Research*, 49(10),  
43 pp. 1037–1044. Available at: <https://doi.org/10.1016/j.visres.2009.01.014>.

44 15) Daw, N.D. et al. (2006) 'Cortical substrates for exploratory decisions in humans',  
45 *Nature*, 441(7095), pp. 876–879. Available at: <https://doi.org/10.1038/nature04766>.

46 16) Dumoulin, S.O. and Wandell, B.A. (2008) 'Population receptive field estimates in  
47 human visual cortex', *NeuroImage*, 39(2), pp. 647–660. Available at:  
48 <https://doi.org/10.1016/j.neuroimage.2007.09.034>.

49 17) Eriksen, C.W. and St. James, J.D. (1986) 'Visual attention within and around the field  
50 of focal attention: A zoom lens model', *Perception & Psychophysics*, 40(4), pp. 225–  
51 240. Available at: <https://doi.org/10.3758/BF03211502>.

52 18) Favila, S.E., Kuhl, B.A. and Winawer, J. (2022) 'Perception and memory have distinct  
53 spatial tuning properties in human visual cortex', *Nature Communications*, 13(1), p.  
54 5864. Available at: <https://doi.org/10.1038/s41467-022-33161-8>.

55 19) Feldmann-Wüstefeld, T. and Awh, E. (2020) 'Alpha-band Activity Tracks the Zoom  
56 Lens of Attention', *Journal of Cognitive Neuroscience*, 32(2), pp. 272–282. Available  
57 at: [https://doi.org/10.1162/jocn\\_a\\_01484](https://doi.org/10.1162/jocn_a_01484).

58 20) Fischl, B. (2012) 'FreeSurfer', *NeuroImage*, 62(2), pp. 774–781. Available at:  
59 <https://doi.org/10.1016/j.neuroimage.2012.01.021>.

60 21) Gobell, J.L., Tseng, C. and Sperling, G. (2004) 'The spatial distribution of visual  
61 attention', *Vision Research*, 44(12), pp. 1273–1296. Available at:  
62 <https://doi.org/10.1016/j.visres.2004.01.012>.

63 22) Greve, D.N. and Fischl, B. (2009) 'Accurate and robust brain image alignment using  
64 boundary-based registration', *NeuroImage*, 48(1), pp. 63–72. Available at:  
65 <https://doi.org/10.1016/j.neuroimage.2009.06.060>.

66 23) Herrmann, K. et al. (2010) 'When size matters: attention affects performance by  
67 contrast or response gain', *Nature Neuroscience*, 13(12), pp. 1554–1559. Available  
68 at: <https://doi.org/10.1038/nn.2669>.

69 24) Hopf, J.-M. et al. (2006) 'The Neural Site of Attention Matches the Spatial Scale of  
70 Perception', *Journal of Neuroscience*, 26(13), pp. 3532–3540. Available at:  
71 <https://doi.org/10.1523/JNEUROSCI.4510-05.2006>.

72 25) Huang, D. et al. (2017) 'The time course of attention modulation elicited by spatial  
73 uncertainty', *Vision Research*, 138, pp. 50–58. Available at:  
74 <https://doi.org/10.1016/j.visres.2017.06.008>.

75 26) Intriligator, J. and Cavanagh, P. (2001) 'The Spatial Resolution of Visual Attention',  
76     *Cognitive Psychology*, 43(3), pp. 171–216. Available at:  
77     <https://doi.org/10.1006/cogp.2001.0755>.

78 27) Itthipuripat, S. *et al.* (2014) 'Changing the Spatial Scope of Attention Alters Patterns  
79     of Neural Gain in Human Cortex', *Journal of Neuroscience*, 34(1), pp. 112–123.  
80     Available at: <https://doi.org/10.1523/JNEUROSCI.3943-13.2014>.

81 28) Jigo, M., Heeger, D.J. and Carrasco, M. (2021) 'An image-computable model of how  
82     endogenous and exogenous attention differentially alter visual perception',  
83     *Proceedings of the National Academy of Sciences*, 118(33), p. e2106436118.  
84     Available at: <https://doi.org/10.1073/pnas.2106436118>.

85 29) Kastner, S. *et al.* (1998) 'Mechanisms of Directed Attention in the Human Extrastriate  
86     Cortex as Revealed by Functional MRI', *Science*, 282(5386), pp. 108–111. Available  
87     at: <https://doi.org/10.1126/science.282.5386.108>.

88 30) Kay, K.N. *et al.* (2013) 'Compressive spatial summation in human visual cortex',  
89     *Journal of Neurophysiology*, 110(2), pp. 481–494. Available at:  
90     <https://doi.org/10.1152/jn.00105.2013>.

91 31) Kiniklioğlu, M. and Boyaci, H. (2022) 'Increasing the spatial extent of attention  
92     strengthens surround suppression', *Vision Research*, 199, p. 108074. Available at:  
93     <https://doi.org/10.1016/j.visres.2022.108074>.

94 32) Klein, B.P., Harvey, B.M. and Dumoulin, S.O. (2014) 'Attraction of Position Preference  
95     by Spatial Attention throughout Human Visual Cortex', *Neuron*, 84(1), pp. 227–237.  
96     Available at: <https://doi.org/10.1016/j.neuron.2014.08.047>.

97 33) Maunsell, J.H.R. (2015) 'Neuronal Mechanisms of Visual Attention', *Annual Review of  
98     Vision Science*, 1(Volume 1, 2015), pp. 373–391. Available at:  
99     <https://doi.org/10.1146/annurev-vision-082114-035431>.

100 34) McAdams, C.J. and Maunsell, J.H. (1999) 'Effects of attention on orientation-tuning  
101     functions of single neurons in macaque cortical area V4', *The Journal of  
102     Neuroscience: The Official Journal of the Society for Neuroscience*, 19(1), pp. 431–  
103     441. Available at: <https://doi.org/10.1523/JNEUROSCI.19-01-00431.1999>.

104 35) McGuire, J.T. *et al.* (2014) 'Functionally Dissociable Influences on Learning Rate in a  
105     Dynamic Environment', *Neuron*, 84(4), pp. 870–881. Available at:  
106     <https://doi.org/10.1016/j.neuron.2014.10.013>.

107 36) McMains, S.A. and Somers, D.C. (2004) 'Multiple Spotlights of Attentional Selection  
108     in Human Visual Cortex', *Neuron*, 42(4), pp. 677–686. Available at:  
109     [https://doi.org/10.1016/S0896-6273\(04\)00263-6](https://doi.org/10.1016/S0896-6273(04)00263-6).

110 37) Moeller, S. *et al.* (2010) 'Multiband multislice GE-EPI at 7 tesla, with 16-fold  
111     acceleration using partial parallel imaging with application to high spatial and  
112     temporal whole-brain fMRI', *Magnetic Resonance in Medicine*, 63(5), pp. 1144–1153.  
113     Available at: <https://doi.org/10.1002/mrm.22361>.

114 38) Müller, N.G. *et al.* (2003) 'A Physiological Correlate of the "Zoom Lens" of Visual  
115 Attention', *Journal of Neuroscience*, 23(9), pp. 3561–3565. Available at:  
116 <https://doi.org/10.1523/JNEUROSCI.23-09-03561.2003>.

117 39) Nadarajah, S. (2005) 'A generalized normal distribution', *Journal of Applied Statistics*,  
118 32(7), pp. 685–694. Available at: <https://doi.org/10.1080/02664760500079464>.

119 40) Nassar, M.R. *et al.* (2010) 'An Approximately Bayesian Delta-Rule Model Explains the  
120 Dynamics of Belief Updating in a Changing Environment', *Journal of Neuroscience*,  
121 30(37), pp. 12366–12378. Available at: <https://doi.org/10.1523/JNEUROSCI.0822-10.2010>.

123 41) Nassar, M.R. *et al.* (2012) 'Rational regulation of learning dynamics by pupil-linked  
124 arousal systems', *Nature Neuroscience*, 15(7), pp. 1040–1046. Available at:  
125 <https://doi.org/10.1038/nn.3130>.

126 42) Nassar, M.R., Bruckner, R. and Frank, M.J. (2019) 'Statistical context dictates the  
127 relationship between feedback-related EEG signals and learning', *eLife*. Edited by  
128 T.H. Donner *et al.*, 8, p. e46975. Available at: <https://doi.org/10.7554/eLife.46975>.

129 43) O'Reilly, J.X. *et al.* (2013) 'Dissociable effects of surprise and model update in parietal  
130 and anterior cingulate cortex', *Proceedings of the National Academy of Sciences*,  
131 110(38), pp. E3660–E3669. Available at: <https://doi.org/10.1073/pnas.1305373110>.

132 44) Palmer, J. and Moore, C.M. (2009) 'Using a filtering task to measure the spatial extent  
133 of selective attention', *Vision Research*, 49(10), pp. 1045–1064. Available at:  
134 <https://doi.org/10.1016/j.visres.2008.02.022>.

135 45) Payzan-LeNestour, E. *et al.* (2013) 'The Neural Representation of Unexpected  
136 Uncertainty during Value-Based Decision Making', *Neuron*, 79(1), pp. 191–201.  
137 Available at: <https://doi.org/10.1016/j.neuron.2013.04.037>.

138 46) Payzan-LeNestour, E. and Bossaerts, P. (2011) 'Risk, Unexpected Uncertainty, and  
139 Estimation Uncertainty: Bayesian Learning in Unstable Settings', *PLOS  
140 Computational Biology*, 7(1), p. e1001048. Available at:  
141 <https://doi.org/10.1371/journal.pcbi.1001048>.

142 47) Posner, M.I. (1980) 'Orienting of Attention', *Quarterly Journal of Experimental  
143 Psychology*, 32(1), pp. 3–25. Available at:  
144 <https://doi.org/10.1080/00335558008248231>.

145 48) Preuschoff, K., 't Hart, B.M. and Einhäuser, W. (2011) 'Pupil Dilation Signals Surprise:  
146 Evidence for Noradrenaline's Role in Decision Making', *Frontiers in Neuroscience*, 5.  
147 Available at: <https://doi.org/10.3389/fnins.2011.00115>.

148 49) Puckett, A.M. and DeYoe, E.A. (2015) 'The Attentional Field Revealed by Single-Voxel  
149 Modeling of fMRI Time Courses', *Journal of Neuroscience*, 35(12), pp. 5030–5042.  
150 Available at: <https://doi.org/10.1523/JNEUROSCI.3754-14.2015>.

151 50) Ress, D., Backus, B.T. and Heeger, D.J. (2000) 'Activity in primary visual cortex  
152 predicts performance in a visual detection task', *Nature Neuroscience*, 3(9), pp. 940–  
153 945. Available at: <https://doi.org/10.1038/78856>.

154 51) Reuter, M., Rosas, H.D. and Fischl, B. (2010) 'Highly accurate inverse consistent  
155 registration: A robust approach', *NeuroImage*, 53(4), pp. 1181–1196. Available at:  
156 <https://doi.org/10.1016/j.neuroimage.2010.07.020>.

157 52) Reynolds, J.H. and Heeger, D.J. (2009) 'The Normalization Model of Attention',  
158 *Neuron*, 61(2), pp. 168–185. Available at:  
159 <https://doi.org/10.1016/j.neuron.2009.01.002>.

160 53) Samaha, J., Sprague, T.C. and Postle, B.R. (2016) 'Decoding and Reconstructing the  
161 Focus of Spatial Attention from the Topography of Alpha-band Oscillations', *Journal*  
162 *of cognitive neuroscience*, 28(8), pp. 1090–1097. Available at:  
163 [https://doi.org/10.1162/jocn\\_a\\_00955](https://doi.org/10.1162/jocn_a_00955).

164 54) Setsompop, K. *et al.* (2012) 'Blipped-controlled aliasing in parallel imaging for  
165 simultaneous multislice echo planar imaging with reduced g-factor penalty',  
166 *Magnetic Resonance in Medicine*, 67(5), pp. 1210–1224. Available at:  
167 <https://doi.org/10.1002/mrm.23097>.

168 55) Shaw, M.L. and Shaw, P. (1977) 'Optimal allocation of cognitive resources to spatial  
169 locations', *Journal of Experimental Psychology: Human Perception and Performance*,  
170 3(2), pp. 201–211. Available at: <https://doi.org/10.1037/0096-1523.3.2.201>.

171 56) Shioiri, S. *et al.* (2016) 'Visual attention spreads broadly but selects information  
172 locally', *Scientific Reports*, 6(1), p. 35513. Available at:  
173 <https://doi.org/10.1038/srep35513>.

174 57) Smith, S.M. *et al.* (2004) 'Advances in functional and structural MR image analysis  
175 and implementation as FSL', *NeuroImage*, 23, pp. S208–S219. Available at:  
176 <https://doi.org/10.1016/j.neuroimage.2004.07.051>.

177 58) Sprague, T.C. and Serences, J.T. (2013) 'Attention modulates spatial priority maps in  
178 the human occipital, parietal and frontal cortices', *Nature Neuroscience*, 16(12), pp.  
179 1879–1887. Available at: <https://doi.org/10.1038/nn.3574>.

180 59) Taylor, J.E.T. *et al.* (2015) 'Attentional cartography: mapping the distribution of  
181 attention across time and space', *Attention, Perception, & Psychophysics*, 77(7), pp.  
182 2240–2246. Available at: <https://doi.org/10.3758/s13414-015-0943-0>.

183 60) Tkacz-Domb, S. and Yeshurun, Y. (2018) 'The size of the attentional window when  
184 measured by the pupillary response to light', *Scientific Reports*, 8(1), p. 11878.  
185 Available at: <https://doi.org/10.1038/s41598-018-30343-7>.

186 61) Tünçok, E., Carrasco, M. and Winawer, J. (2024) 'Spatial attention alters visual  
187 cortical representation during target anticipation'. bioRxiv, p. 2024.03.02.583127.  
188 Available at: <https://doi.org/10.1101/2024.03.02.583127>.

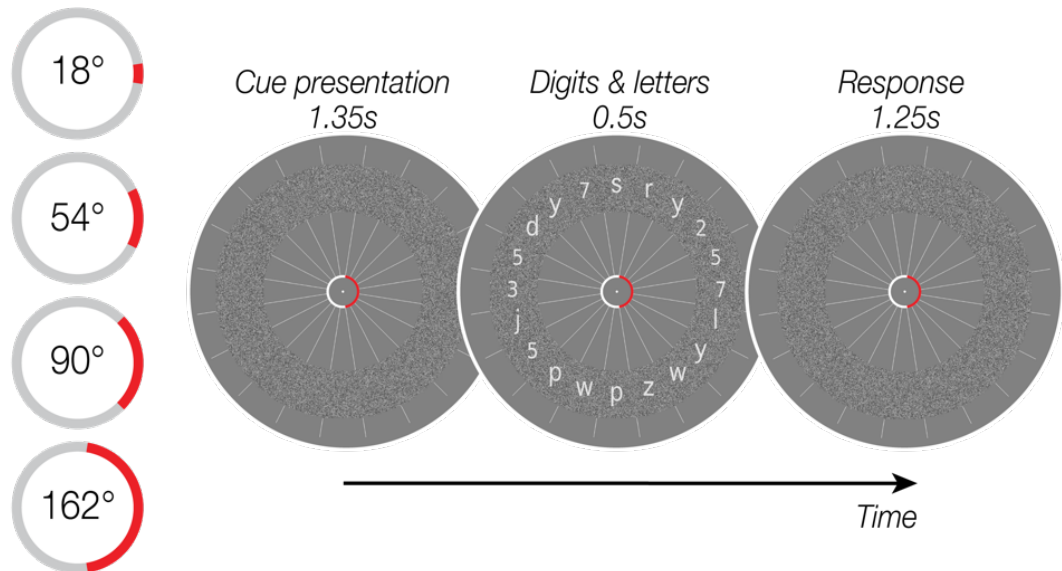
189 62) Vo, V.A., Sprague, T.C. and Serences, J.T. (2017) 'Spatial Tuning Shifts Increase the  
190 Discriminability and Fidelity of Population Codes in Visual Cortex', *Journal of*  
191 *Neuroscience*, 37(12), pp. 3386–3401. Available at:  
192 <https://doi.org/10.1523/JNEUROSCI.3484-16.2017>.

193 63) Yeshurun, Y. (2019) 'The spatial distribution of attention', *Current Opinion in  
194 Psychology*, 29, pp. 76–81. Available at:  
195 <https://doi.org/10.1016/j.copsyc.2018.12.008>.

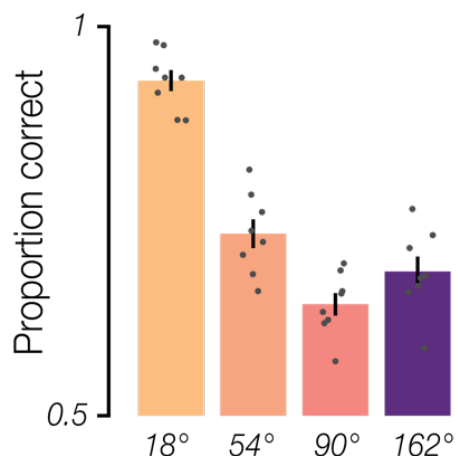
196

**Figure 1.**

*a. Attention task trial sequence*



*b. Behavioral task performance*



*c. Gaze distance from fixation*

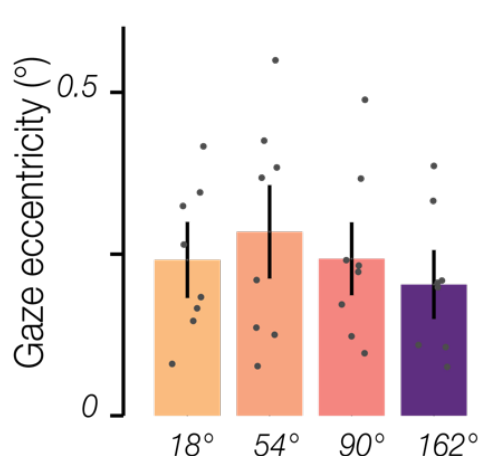
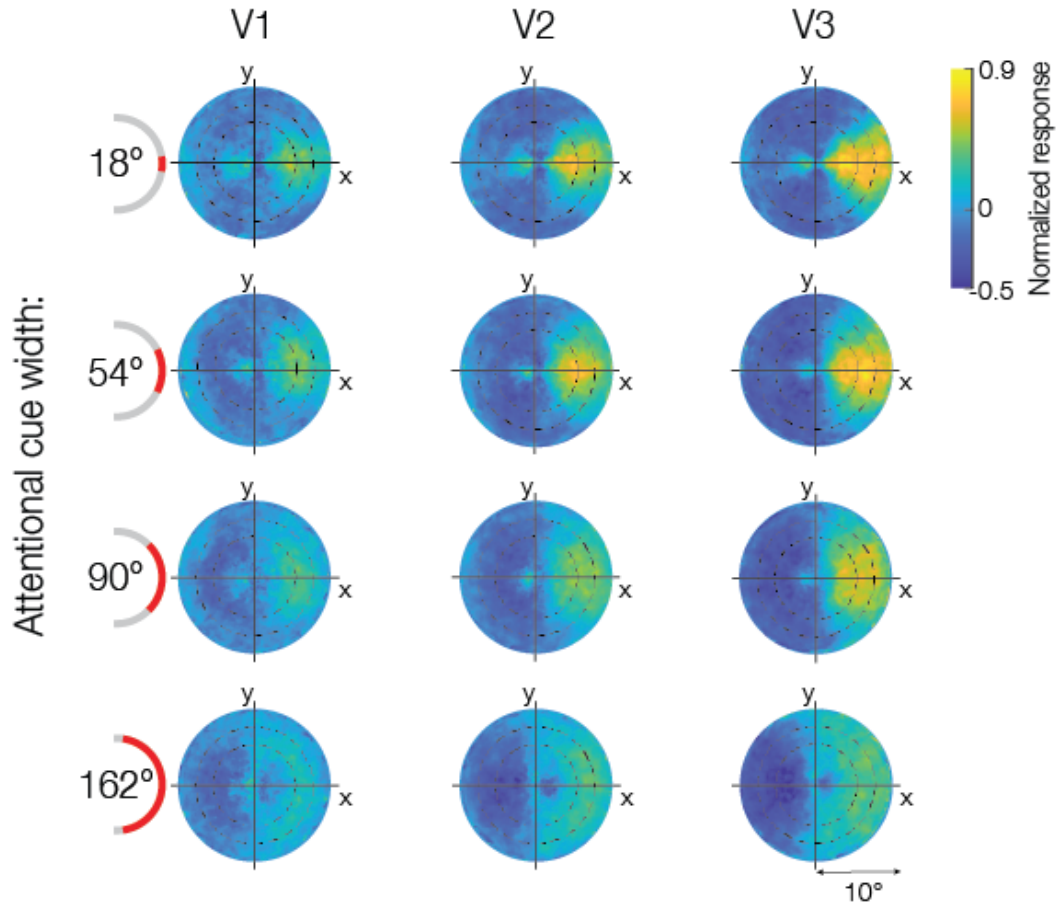


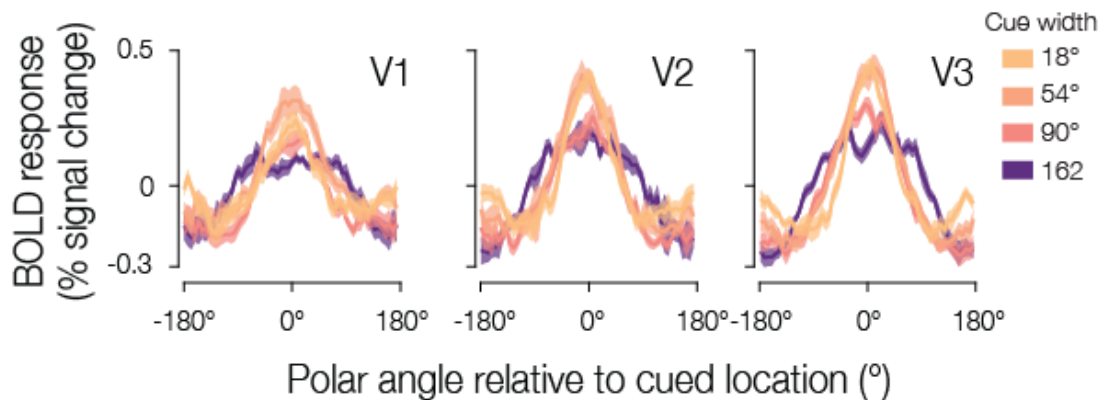
**Figure 1. a.** Task schematic. Participants were instructed to maintain central fixation and use covert spatial attention to determine whether there were more numbers or letters present within a cued region of a white noise annulus. On each trial, the red cue was displayed alone for 1.35 s and remained present throughout the trial. Twenty digits and letters were then presented for 0.5 s, equally spaced and overlaid on the annulus. Participants had 1.25 s to indicate via button press whether more digits or letters were present in the cued region. The cue remained stable for 5 trials (10 TRs, 15.5 s), had a width of 1, 3, 5, or 9 segments (18°, 54°, 90°, or 162°), and was centered on any of the 20 digit/letter slots. **b.** Behavioral task performance: Group mean accuracy for each cue width. Error bars are SEM; gray circles show individual participants. **c.** Group mean gaze eccentricity (in degrees of visual angle) for each cue width, conventions as in **b**.

**Figure 2**

*a. Attention: 2D BOLD activity reconstruction*



*b. Spatial profile attentional modulation*



response projected into the visual field for each attentional cue width. Heatmaps represent the group mean BOLD activity using each voxel's population receptive field (pRF) location within the visual field, shown separately for V1, V2, and V3. Maps were rotated to align all attentional cue locations to 0° polar angle (rightward). Concentric circles indicated by black dashed lines represent the location of the white noise annulus. **b.** Average spatial modulation profiles at the eccentricity of the annulus. The spatial profiles were recentered to 0° polar angle based on the cue location. Solid lines represent the group mean BOLD response and shaded regions the SEM across participants.

**Figure 2.**  
**a. BOLD**

**Figure 3**

*a. Generalized Gaussian model   b. Quantify attentional field*

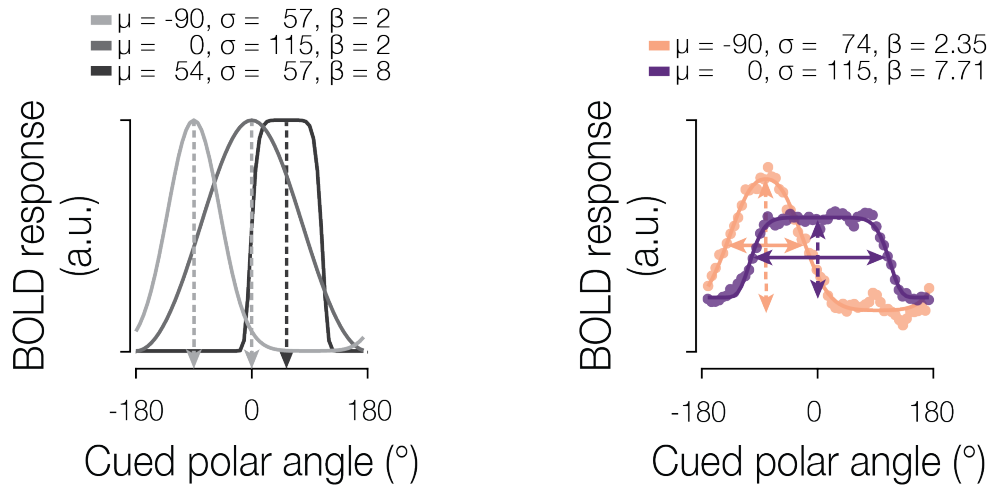


**Figure 3. a.** Modeling approach. The generalized Gaussian model is characterized by parameters for location ( $\mu$ ), scale ( $\sigma$ ), and shape ( $\beta$ ). **b.** Example model fits for two spatial profiles. Dots indicate BOLD response for two attentional cues differing in position and width. Solid lines indicate the best fitting model estimate. To quantify the attentional field, we extracted the location and gain (dashed arrows), as well as the width (FWHM; solid arrows).

**Figure 4.**

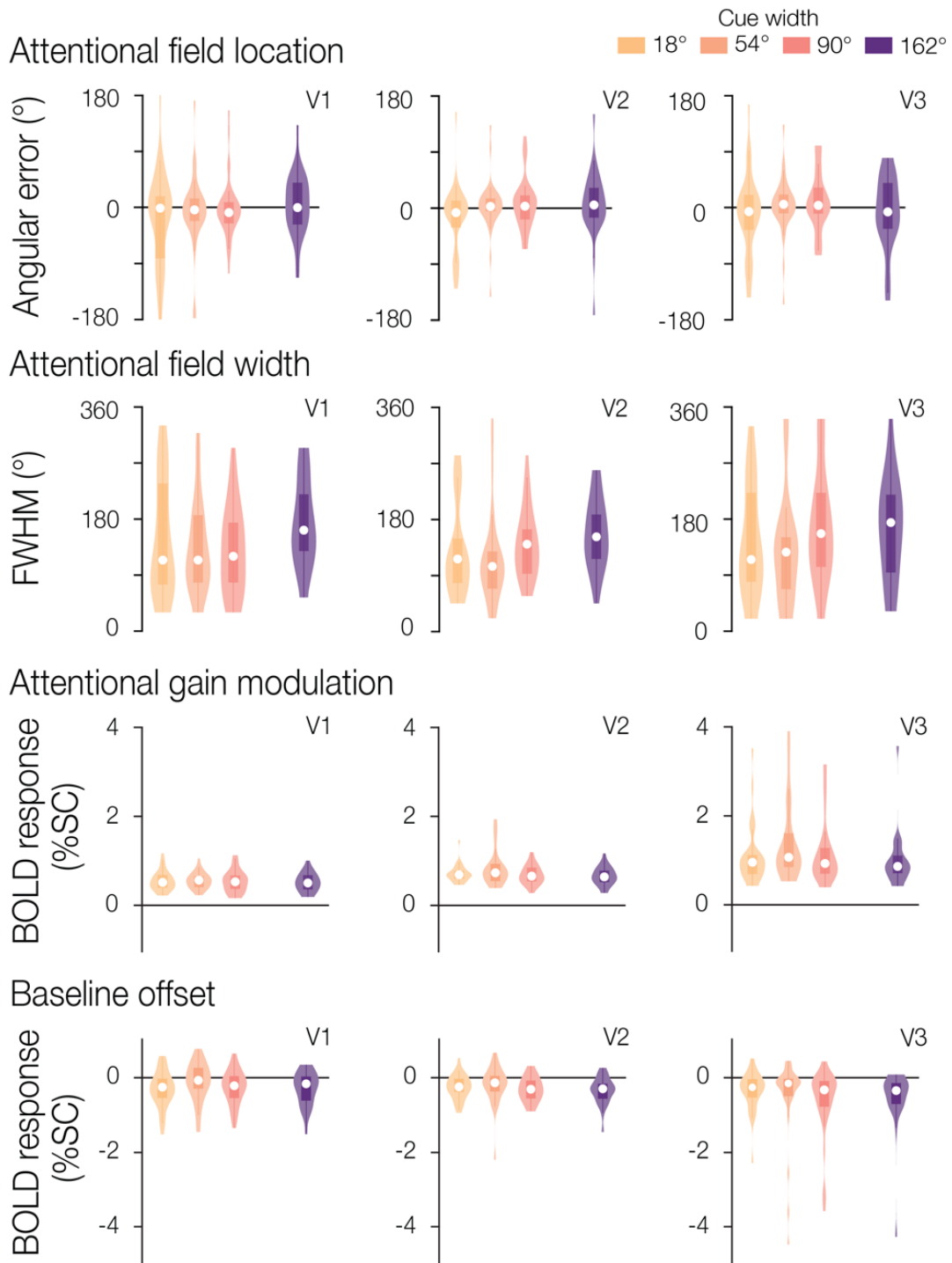
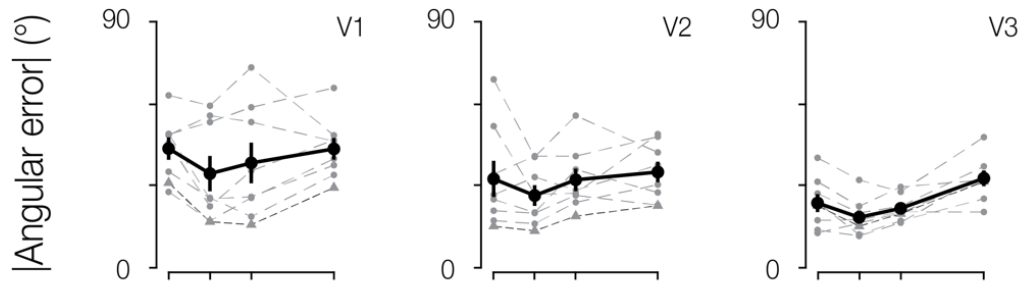


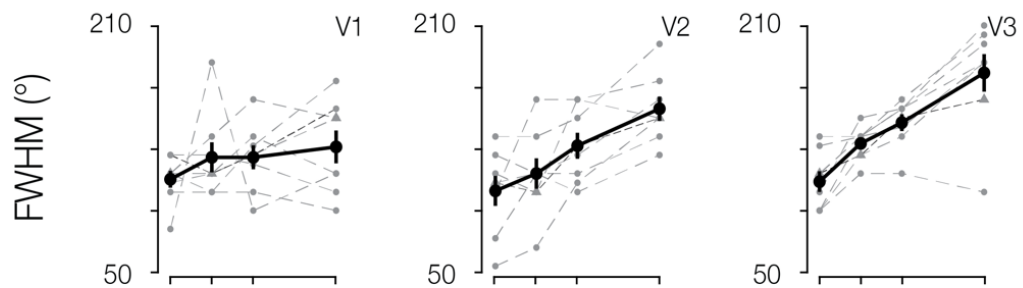
**Figure 4.** Attentional field parameter estimates for an example participant. The full parameter estimate distributions across blocks for location, width, gain, and baseline are shown for one example participant in V1, V2, and V3. Median parameter estimates are shown by the white points, with the box plot representing the 25th to 75th percentile, and whiskers extending to all non-outlier points.

**Figure 5.**

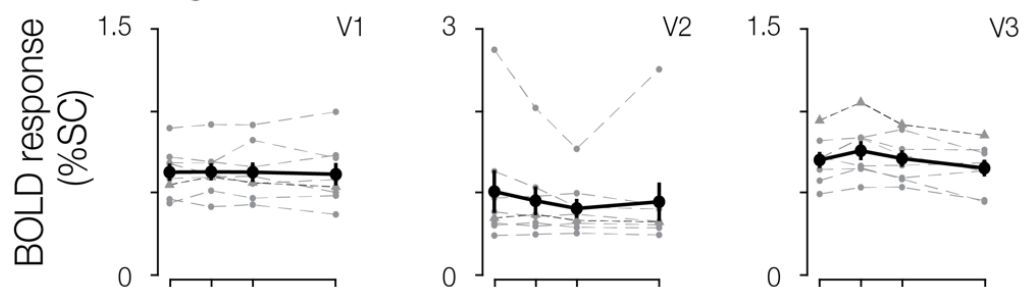
Attentional field location



Attentional field width



Attentional gain modulation



Baseline offset

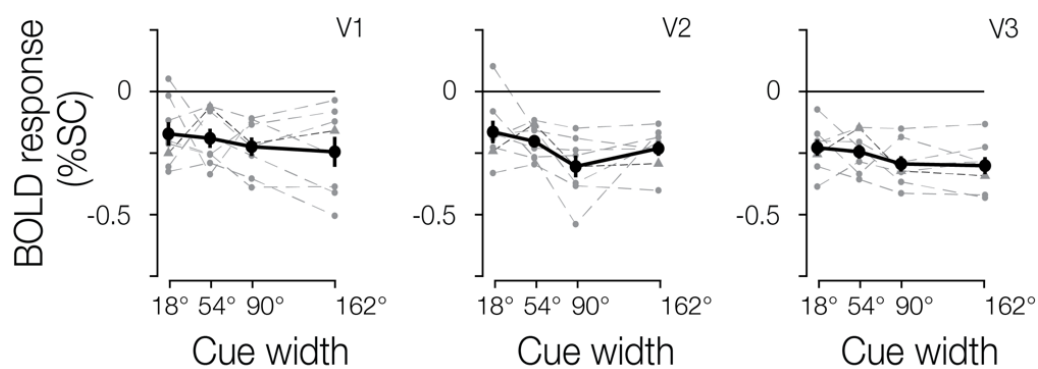


**Figure 5.** Attentional field parameter estimates. Group results for location, width, gain, and baseline estimates. Overall group mean and standard error are shown in solid black, separated by cue width and brain region. Individual participant median estimates are shown in grey. The example participant from Figure 4 is indicated by a denser dashed dark gray line with triangle symbols to aid in comparison.

**Figure 6.**

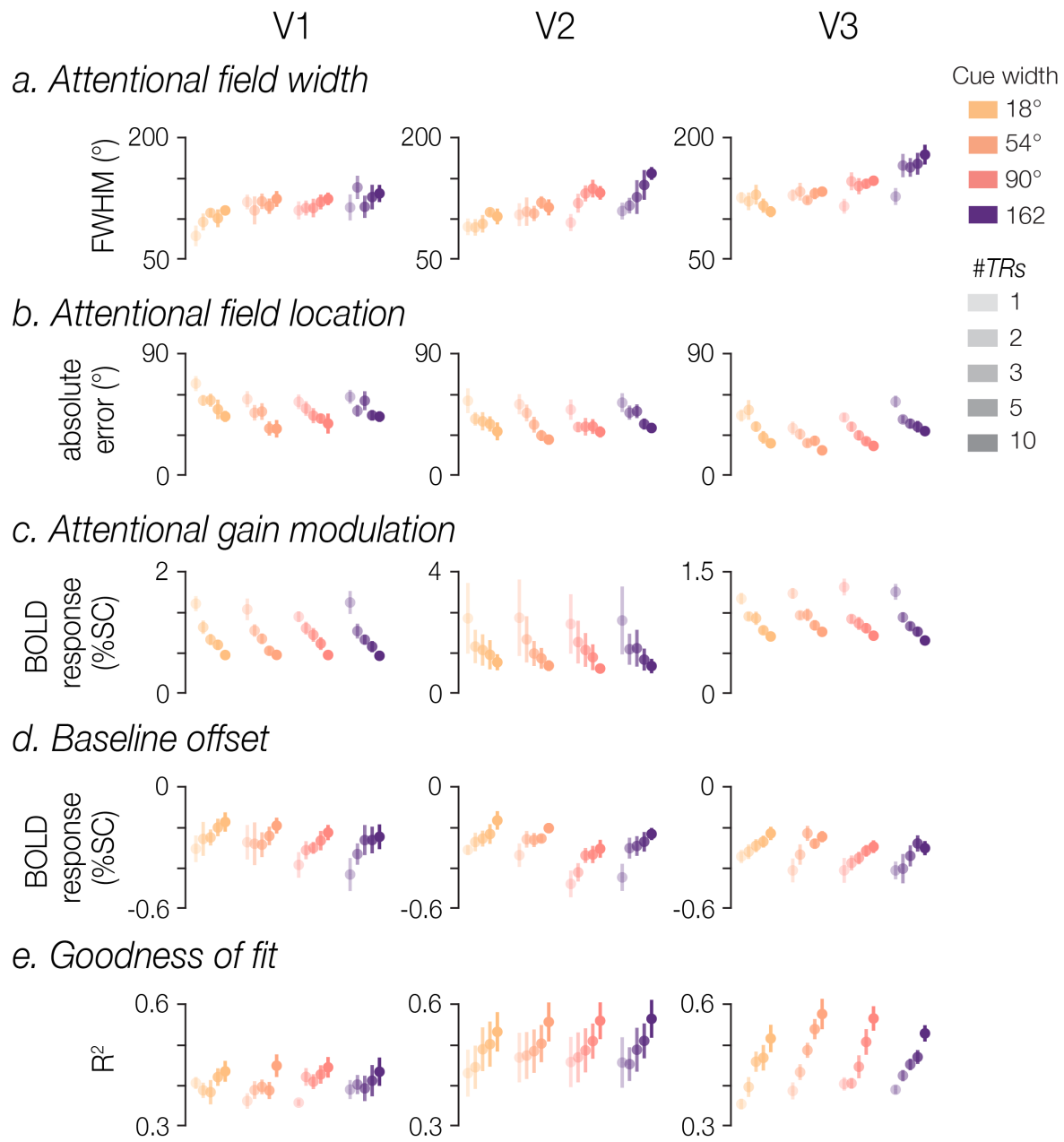
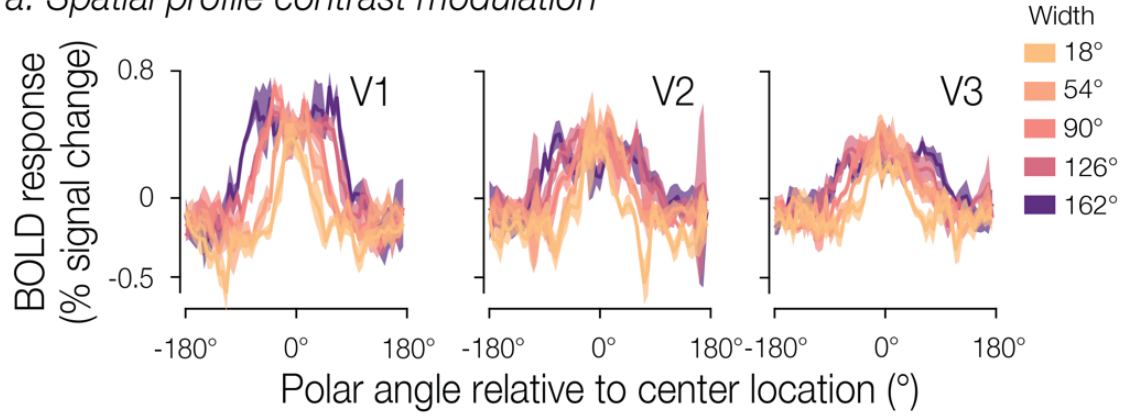


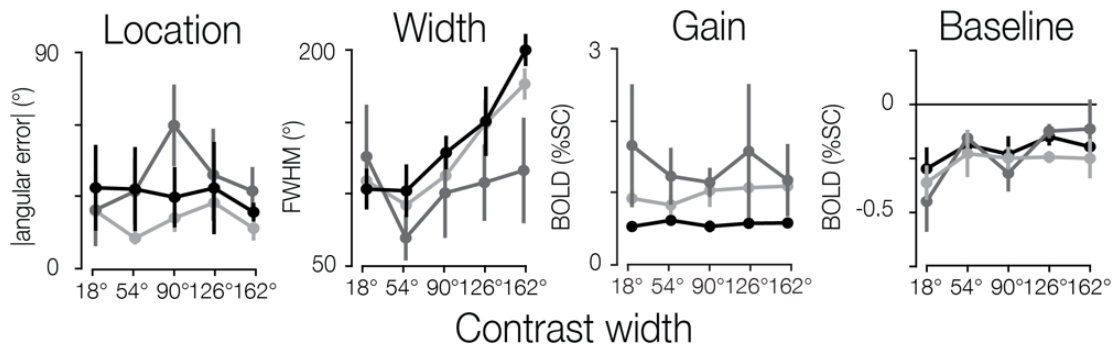
**Figure 6.** Effect of number of TRs. Model fits were computed using BOLD data averaged across different temporal intervals (1, 2, 3, 5, or 10 TRs). Group means (with SEM) are plotted for FWHM, absolute angular error, gain, baseline estimates, and  $R^2$ , separated by cue width, brain region, and the number of TRs used for each model fit.

**Figure 7.**

*a. Spatial profile contrast modulation*



*b. Group results*



*c. FWHM comparison*

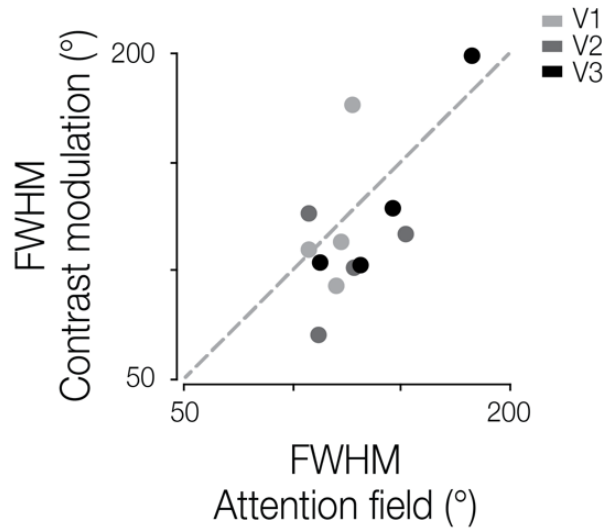


**Figure 7. a.** Spatial profiles of perceptual modulation. Solid lines represent the group mean BOLD activity and shaded regions the SEM. **b.** Group level parameter estimates. Overall group mean and standard error are shown for the absolute angular error, FWHM, gain and baseline, separated by contrast width and brain region. **c.** Comparison of FWHM estimates obtained from the attentional manipulation and the physical contrast manipulation. Dot color indicates brain region; each point represents the mean FWHM for a given width condition across participants.